Pyrite Oxidation in Acid Mine Drainage Systems: Oxygen Isotope Systematics of Intermediate Sulfoxyanions in Sociopolitical Context

A Thesis Presented

by

Madison Liana Goldberg

to

The Department of Earth and Planetary Sciences

in partial fulfillment of the requirements
for a degree with honors
of Bachelor of Arts

April 2021
Harvard College

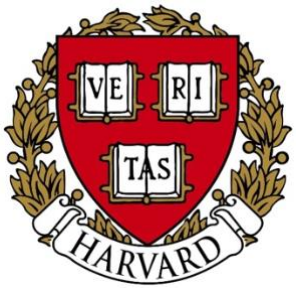

ABSTRACT

Acid mine drainage (AMD) is a widespread and persistent environmental threat in the United States, affecting ecosystems at all trophic levels and endangering human health. Produced by the oxidation of sulfide minerals exposed to the atmosphere during mining and construction projects, AMD is characterized by acidic runoff containing high concentrations of dissolved sulfate and heavy metals. Although AMD impacts watersheds from coast to coast, its effects are not evenly distributed and tend to mirror socioeconomic and racial inequities.

This thesis attempts to investigate both the sociopolitical and scientific dimensions of this issue. The preface considers the ways in which AMD affects Indigenous communities, focusing specifically on the Navajo Nation; primary- and secondary-source research, as well as interviews with stakeholders, indicate that the prevalence of AMD in these communities reflects a long history of structural inequities faced by Indigenous peoples in the U.S. Against that backdrop, the majority of the thesis investigates an unresolved dimension of the mechanism by which pyrite – the most abundant metal sulfide in the Earth's crust and the primary contributor to AMD – oxidizes. Specifically, the precise roles of the aqueous intermediate sulfoxyanions sulfite (SO_3^{2-}) and thiosulfate ($S_2O_3^{2-}$) remain a subject of debate. This work aims to constrain the prevalence and isotope systematics of these species and apply those results to a mining-influenced environment.

It is found that sulfite and thiosulfate make up a notable proportion of the aqueous sulfoxyanion pool at circumneutral or high pH, particularly under oxic conditions. The equilibrium oxygen isotope fractionation factor $^{18}\varepsilon_{SO_3\text{-}H_2O}$ of the sulfite-water system at 22°C is determined to range from 9.76‰ at pH 2 to 7.64‰ at pH 10, with a clear dependence on speciation within the sulfite system. The equilibrium oxygen isotope fractionation factor $^{18}\varepsilon_{S_2O_3\text{-}}$

$_{H_2O}$ for the thiosulfate-water system is also reported at 22°C (ranging from 22.11‰ at pH 2 to 14.67‰ at pH 10), as well as at 4°C (23.93‰ at pH 2 to 14.74‰ at pH 10) and at 93°C (13.02‰ at pH 7 and 14.25‰ at pH 10; thiosulfate appeared to have decomposed at 93°C and pH 2). Measured $^{18}\varepsilon_{S_2O_3\text{-}H_2O}$ at pH 2 (22°C and 4°C) was in good agreement with theoretical predictions presented by Hemingway et al. (in preparation). Based on those predictions, the thiosulfate-water system appeared not to have reached oxygen isotopic equilibrium at higher pH values, suggesting that the rate of oxygen isotope exchange between these two species is pH-dependent. Given that interpretation, the reliability of the $^{18}\varepsilon_{S_2O_3\text{-}H_2O}$ values calculated for pH 7 and 10 at all temperatures is considered to be limited.

The isotope systematics constrained by these experiments are ultimately applied to samples from a natural environment affected by a former gold mine, in order to constrain the specific pathways by which sulfate has formed via pyrite oxidation. The oxygen isotopic composition of these environmental samples ranges widely, and comparison with the isotopic equilibrium data suggests that multiple pathways involving both H_2O and O_2 as donors of a fourth oxygen atom are involved in the production of sulfate at these sites. The combined results of this work, therefore, suggest that AMD prevention strategies should target multiple sulfate formation pathways if they are to be effective.

TABLE OF CONTENTS

LIST OF FIGURES

LIST OF TABLES

ACKNOWLEDGEMENTS

I am very grateful to David Johnston, Andrew Knoll, and Jordon Hemingway for their excellent mentorship and advising throughout my senior thesis, and to all members of the Johnston Lab for their support during this project. I would also like to thank Esther James and Annika Quick for their instruction and feedback during EPS 99A and 99B. Furthermore, I am very grateful to Prentiss Balcom and Bridger Ruyle (Harvard University, Cambridge, MA, USA) for conducting the IC analyses; Magdalena Osburn (Northwestern University, Evanston, IL, USA) for providing fluid samples from the Deep Mine Microbial Observatory in Lead, South Dakota; Daniel Montluçon and Reto Wijker (Geological Institute, ETH Zürich, Zürich, Switzerland) for performing the N_2-BET analysis; Dirk Sachse and Oliver Rach (GFZ German Research Centre for Geosciences, Potsdam, Germany) for conducting oxygen isotopic analysis of laboratory water; and Nir Galili (Weizmann Institute of Science, Rehovot, Israel) for synthesizing the hematite used in this work.

The preface to this work would not have been possible without the generosity of those who shared their experiences and knowledge with me during our interviews: Chris Shuey (Southwest Research and Information Center, Albuquerque, NM, USA); Johnnye Lewis (University of New Mexico, Albuquerque, NM, USA); Karletta Chief (University of Arizona, Tucson, AZ, USA); Erin Savage (Appalachian Voices, Boone, NC, USA); and Rachel Pell (West Virginia Water Research Institute, Morgantown, WV, USA). I am also grateful to Teracita Keyanna (Multicultural Alliance for a Safe Environment, Albuquerque, NM, USA) and Jeff Gaco (Pueblo of Laguna, Laguna, NM, USA) for sharing their stories during a recent panel at the Harvard University Belfer Center for Science and International Affairs, titled “Living with Uranium: The Impact of Uranium Mining on Indigenous Communities.”

Uranium and hardrock mining on Indigenous land in the United States – as well as the forced removal, treaty abrogation, and disinvestment that enabled and enables it – has created an ongoing environmental and public health crisis in these communities. Abandoned mines and acid mine drainage affect the ancestral homelands and water resources of many tribes in the western United States, including the Diné (Navajo) in Utah, Arizona, and New Mexico; the bands of the Oceti Sakowin (Sioux) in South Dakota; and the Northern Arapaho and Eastern Shoshone in Wyoming. In particular, the environmental samples analyzed in this work come from the former Homestake Gold Mine in Lead, South Dakota. Over the period of its operation (from 1876 to 2001), the mine released large amounts of arsenic into the Cheyenne River; the floodplains surrounding the Cheyenne River Sioux Tribe Reservation remain contaminated to this day, potentially exposing residents to toxicity via traditional forms of land use (Lewis et al., 2017). In other words, the samples used in this thesis are connected to a long and painful history of degradation and extraction on Indigenous land, and I engage in analysis of these samples with this history in mind.

To learn more about this history, please visit the websites of the Diné (https://www.navajo-nsn.gov/); the Cheyenne River Sioux (https://www.cheyenneriversiouxtribe.org/); the Northern Arapaho (http://northernarapaho.com/wp/); and the Eastern Shoshone (https://easternshoshone.org/).

PREFACE

"Over a Hundred Years and Several Generations":
Abandoned Hardrock Mines and the Navajo Nation

Note: Members of the Navajo Nation refer to themselves as Diné, meaning "The People." In this chapter, I will refer to the political entity as the Navajo Nation, as that is how it is officially recognized by the tribal government, but I will refer to its members as Diné.

In the summer of 1970, David Shaw was in high spirits. As president of the United Nuclear Corporation, or UNC, he had good news to deliver to the stockholders assembled in the Waldorf-Astoria Hotel: business was – or at least it soon would be – booming. "Ultimately nuclear electric power is going to grow tremendously," he said, according to the following day's issue of the *New York Times.*[1] "When everybody finally understands it all, environmentalists will insist on nuclear power. I think we can really say, 'What is good for the environment is good for United Nuclear.'"

Nine years later, almost to the day, a dam failed at one of United Nuclear Corporation's uranium mills, unleashing the largest liquid radioactive spill in U.S. history. The mill processed ore from the country's largest underground uranium mine – also operated by United Nuclear – located near Church Rock, New Mexico (called *Kinlitsosinil* in Diné), and bordered by the Navajo Nation.[2] The dam had protected a waste impoundment filled with tailings, toxic leftovers from the uranium extraction process, and when it broke, an estimated 94 million gallons of contaminated fluid and 1,100 tons of radioactive solid waste escaped. According to a government report on the incident, a smaller emergency dam stopped most of the solid waste, but

[1] "United Nuclear Corp. Foresees a Rise in Need for Power Plants," *New York Times*, July 18, 1970, 32, ProQuest.
[2] Doug Brugge, Jamie L. deLemos, and Cat Bui, "The Sequoyah Corporation Fuels Release and the Church Rock Spill: Unpublicized Nuclear Releases in American Indian Communities," *American Journal of Public Health* 97, no. 9 (2007): 1595-1600. https://doi.org/10.2105/AJPH.2006.103044.

the hazardous liquid surged through Pipeline Arroyo and into the Rio Puerco.[3] The waste traveled 100 miles downstream and into Arizona, contaminating Navajo grazing lands in the process.[4]

The spill's exact health implications for people living in the region (almost all Diné farmers) remain murky to this day. In a congressional hearing months after the dam failure, representatives for United Nuclear presented measurements which suggested that, shortly following the spill, heavy rain had diluted radioactivity in the soil, air, and water to background levels.[5] But subsequent environmental studies have proven worryingly inconsistent. Measurements of radioactivity taken by the operator of the United Nuclear mill were completely different from – and consistently far lower than – those reported by the State of New Mexico.[6] The six people brought to Los Alamos Scientific Laboratory for exposure testing were deemed unaffected, but experts have argued that those findings hold little weight: there were no controls or prior radiation levels to use for comparison, and there was no plan to monitor the individuals for potential long-term effects of exposure.[7] And in the areas where testing did show elevated levels of radiation, as in livestock tissue, government guidance lacked clarity and direction. According to congressional testimony by Helen George, a Diné member of the Church Rock Action Committee, Diné farmers were told not to eat their livestock; they were not, however, informed how long they should wait, and their requests for emergency food stamps in the absence of a traditional food source were summarily denied.[8]

---

[3] New Mexico Environmental Improvement Division, "The Church Rock Uranium Mill Tailings Spill: A Health and Environmental Assessment," Santa Fe, New Mexico, Sept. 1983.
[4] U.S. Congress, House of Representatives, Committee on Interior and Insular Affairs, *Mill Tailings Dam Break at Church Rock, New Mexico*, 96th Congress, 1st sess., 1979, 1.
[5] *Ibid.*
[6] *Ibid.,* 11.
[7] *Ibid.,* 18.
[8] *Ibid.,* 14.

Ultimately, whatever the damage caused by the spill itself, it quickly became clear that the 1979 breach was only the tip of a uranium-laden iceberg. Because many of the uranium mines in the area were excavated below the water table, operators had to continuously remove groundwater that seeped in, a process called "dewatering"; for years, uranium mines had been pumping 5,000 gallons per minute of dewatering discharge into the Rio Puerco.[9] Mine operators did not start treating this water until the mid-1970s, and even once they had introduced partial treatment systems, radioactivity and toxic metal concentrations remained high: levels of thorium-230, polonium-210, selenium, lead, arsenic, and molybdenum were sufficiently elevated that, in 1983, the New Mexico Environmental Improvement Division recommended restrictions on the use of surface water and groundwater in the region.[10] That same year, noting the continuing toxic discharge into the Rio Puerco, the Environmental Protection Agency added the Church Rock site to its National Priorities List – the list of U.S. areas so contaminated by industry that they are candidates for federal oversight as part of the Superfund cleanup program.[11]

The Church Rock spill, therefore, drew a measure of short-lived attention to a pervasive environmental and human health threat on and around Navajo land. As Frank Paul, vice chairman of the Navajo Tribal Commission, explained at the congressional hearing: "The UNC incident does not exist in a vacuum. We Navajos have already had to contend with abandoned mines, mills, and tailings" scattered throughout a number of states in the American Southwest.[12] In fact, the Church Rock spill provides an informative case study of the much larger sociopolitical dynamics behind mining practices in the region. For instance, the chaotic response to the dam failure reflects a long-standing crisis of responsibility when it comes to governmental

[9] New Mexico EID, "The Church Rock Uranium Mill Tailings Spill," 1.
[10] *Ibid.*, 29-32.
[11] Brugge et al., "The Sequoyah Corporation Fuels Release and the Church Rock Spill."
[12] U.S. Congress, House of Representatives, *Mill Tailings Dam Break*, 6.

protection of Indigenous territory: a jurisdictional quagmire created by a long history – carried out by the federal government and private corporations – of dividing, allocating, leasing, and exploiting Indigenous land, often with little tribal community involvement. Helen George, the Church Rock Action Committee member, described the issue in her testimony: "Part of the problem with trying to deal with this incident is the varying land status in our area. The people do not understand the different types of land in the checkerboard area…How can the Navajo Tribe protect its citizens if these jurisdictional problems are not answered, and if nothing is done about these problems?"[13]

What's more, both United Nuclear Corporation and the government agencies tasked with monitoring it have been charged with outright negligence in the case of the Church Rock spill. As Representative Morris Udall of Arizona, the chairman of the House subcommittee holding the hearing, pointed out, an engineering consultant for United Nuclear predicted – *before* the dam was approved or built – that the soil underneath it was "susceptible to extreme settling which was likely to cause the cracking and subsequent failure of the structure."[14] It remains unclear whether that instability caused the dam failure in 1979. It is notable, however, that three separate regulatory agencies had this information in hand when they licensed the dam without any "detailed independent assessments" of its construction – and when the dam started to crack in 1977, two years before the spill, United Nuclear did not report the problem.[15]

These errors – at best, willful ignorance and at worst, genuine malfeasance – reflect a disregard for the people living on this land and a collective willingness to turn a blind eye to the harm suffered as hardrock mining proliferated. As Frank Paul said in his testimony, "What is

[13] *Ibid.*, 15.
[14] *Ibid.*, 2.
[15] *Ibid.*, 2-3.

disturbing to me, and what is disturbing to the communities of the Navajo Nation which are presently dealing with the uranium industry, is that our country knew better. Research into the problems of uranium and radiation had been going on for many, many years."[16] Nonetheless, he says, "…the Navajo Nation was taken for granted as some kind of proving ground or national sacrifice area in which the defense and energy needs of the United States would be given priority, but the health and safety and long-term economic needs of the Navajo people were ignored."[17] The inattention did not disappear with the Church Rock spill. Even after the disaster, public concern was conspicuously scarce. As Paul pointed out in the hearing before the House, "…while we appreciate this committee's interest and concern, we do note that a smaller incident at Three Mile Island commanded a Presidential Commission. Yet today's hearing represents the first serious national concern for this incident, and it is now over three months since the dam failed."[18]

The mine pollution problem in the American West has deep roots. This section will draw on primary- and secondary-source research, as well as firsthand accounts from stakeholders, to investigate the modern dimensions of this issue and its implications for Diné communities in particular. An array of social, political, and economic forces has shaped the water quality crisis that has resulted from hardrock mining on Indigenous land in the United States. As a result, acid mine drainage – the issue that my lab research targets – is inextricable from its sociopolitical context; the chemical changes taking place at the microscopic level fuel a sprawling environmental and public health problem. In this section, I explore that problem and what it

[16] *Ibid.*, 8.
[17] *Ibid.*, 7.
[18] *Ibid.*, 6.

means for the people who live, work, and play in landscapes fundamentally altered by hardrock mining.

U.S. Hardrock Mining and Its History

In 2020, the Government Accountability Office (GAO) issued a report on abandoned mines in the western United States.[19] According to the GAO, the four federal agencies with a hand in mine management – the Forest Service, the Bureau of Land Management, the National Park Service, and the Environmental Protection Agency – had identified 140,000 abandoned hardrock mine features (a tunnel or a tailings pile, for example) on federal land by the time of the report. The list is limited to thirteen western states, but the GAO points out that these states house the majority of the country's abandoned hardrock mines – and with New Mexico, Arizona, and Utah all included, the Navajo Nation is firmly situated in this region of greatest concern. Of those 140,000 mine features, 67,000 pose hazards to physical safety, and 22,500 present environmental hazards; what's more, the agencies estimated that more than 390,000 abandoned hardrock mine features remain unidentified throughout the western U.S.[20]

It is no coincidence that hardrock mines – which produce metals such as gold, copper, and uranium – are concentrated on Indigenous land. Through a succession of legislation and treaties – and, often, unilateral abrogation of those treaties by Congress – the United States government has appropriated most tribal land for its own use, either by declaring those lands open to industrial development or by claiming ownership entirely.[21] The roots of these practices extend back to the colonial period, when European settlers cited what they termed the "principle

[19] Government Accountability Office, "Abandoned Hardrock Mines," Washington, DC, March 5, 2020. https://www.gao.gov/products/gao-20-238.
[20] *Ibid.*
[21] Mike Townsend, "Congressional Abrogation of Indian Treaties: Reevaluation and Reform," *Yale Law Review* 98, no. 4 (1989): 793-812. https://www.jstor.org/stable/796733.

of discovery" as a justification for seizing whatever tribal lands they came upon.[22] By the mid-nineteenth century, the U.S. government had designated as "public land" almost all Indigenous territory, and it assumed the power to return portions of that land to the tribes in the form of reservations.[23] The amount of land under tribal control shrank rapidly, as these reservations amounted to mere slivers of the original territory occupied by Indigenous peoples, but one of the most dramatic reductions came in the decades following 1887, after Congress passed the General Allotment Act. This law, which assigned small parcels of land to each family in a given tribe and reserved the rest for sale by the government, would cause tribes to lose two-thirds of the land that had been under their control at the time of the law's passage.[24] It also created a landscape that was both physically and legally fragmented: the jurisdictional "checkerboard" that Helen George would describe decades later in the hearing on the Church Rock spill.

The federal government's goal was often to move tribal communities westward, to make the productive land in the eastern United States available for development by non-Indigenous settlers. The Indian Removal Act, for instance, was an 1830 law whose full title was "An Act to provide for an exchange of lands with the Indians residing in any of the states or territories, and for their removal west of the river Mississippi."[25] As a result of this law and others like it, 93% of reservation land in the country is situated in eleven states in the western U.S., plus South Dakota.[26]

---

[22] Klaus Frantz, *Indian Reservations in the United States: Territory, Sovereignty, and Socioeconomic Change* (Chicago: University of Chicago Press, 1999), 39-40.
[23] *Ibid.*, 45.
[24] *Ibid.*, 40.
[25] The Library of Congress, "A Century of Lawmaking for a New Nation: U.S. Congressional Documents and Debates, 1774-1875: Statutes at Large, 21st Congress, 1st Session," *LOC American Memory*, https://memory.loc.gov/cgi-bin/ampage?collId=llsl&fileName=004/llsl004.db&recNum=458, accessed Feb. 2021.
[26] Frantz, *Indian Reservations*, 41.

Lawmakers originally considered western land ideal for reservations, since it was less agriculturally productive than land east of the Mississippi and therefore seemed comparatively useless.[27] Once the federal government became aware of the rich mineral resources in western regions, however, legislative priorities changed dramatically. William Jones, the U.S. Indian Affairs Commissioner, declared in 1902 that reservation land ought to be "thrown open as rapidly as possible" to make room for mineral extraction.[28] In 1919, Congress passed a law toward that end, declaring that the federal government could lease tribal land to a U.S. citizen or corporation intending to search for "deposits of gold, silver, copper, and other valuable metalliferous minerals."[29] Mining activity has since proliferated on and adjacent to Indigenous land, the product of a tangled history of laws and treaties, which – even when they were not broken – were typically most beneficial to extractive industries and land speculators, as the price of undeveloped, annexed territory was slashed.

The Modern Landscape

A number of metals, including gold, copper, lead, and vanadium – and, with the advent of nuclear weaponry in the mid-twentieth century, uranium – have been mined on the tribal lands of the American west, and on the Navajo Nation in particular.[30] According to a 2017 analysis, an estimated 600,000 Indigenous people live within ten kilometers of an abandoned hardrock mine, out of 4.1 million in the western United States.[31] Uranium mines are especially concentrated,

[27] *Ibid.*, 41.
[28] Johnnye Lewis, Joseph Hoover, and Debra MacKenzie, "Mining and Environmental Health Disparities in Native American Communities," *Current Environmental Health Reports,* 4 (2017): 130-141, https://doi.org/10.1007/s40572-017-0140-5.
[29] U.S. Congress, *Public Laws of the Sixty-Sixth Congress*, 66th Congress, Sess. 1, 1919, Ch. 4.
[30] Traci Brynne Voyles, *Wastelanding: Legacies of Uranium Mining in Navajo Country* (Minneapolis: University of Minnesota Press, 2015).
[31] Lewis, "Mining and Environmental Health Disparities," 131.

with 20% located within ten kilometers of a reservation and 75% within 80 kilometers – even though reservation land makes up only 5.6% of the western U.S.[32]

Although the last uranium mine on Navajo land closed in the mid-1980s, the health and environmental legacies of its extraction remain pervasive. "The abandoned mines are in all four directions: east, west, south, north, and in the middle of the Navajo Nation," says Chris Shuey, an environmental health specialist with the Southwest Research and Information Center. Out of 110 chapters, the units of local governance on the Navajo Nation, Shuey says that his team counted 57 – more than half – with at least one major source of uranium exposure. Despite the sprawling scope of the problem, however, research on the implications of abandoned mines for adjacent communities remained sluggish. According to Shuey, the topic was rarely investigated when he turned his attention to mine waste issues in the 1970s. "Anybody who questioned the role of uranium mining and processing in population health effects was branded an antinuclear zealot," he says. He and his team finally received their first grant to study the issue in 2002, almost twenty years after the last uranium mine closed. "We were two to three decades behind in studying the health effects at the population level, and we are still decades behind in actually doing the remediation."

Meanwhile, the abandoned mines have become a treacherous fact of life for those living on the Navajo Nation. Teracita Keyanna, a Diné woman who lives in the Red Water Pond Road community, spoke recently as part of a panel on the legacy of uranium mining on Indigenous land.[33] "We are a small community sandwiched between two uranium mines and half a mile from a uranium mill," she said. That mill is Church Rock, and Keyanna remembers when the

[32] *Ibid.*, 135.
[33] Teracita Keyanna, "Living with Uranium: The Impact of Uranium Mining on Indigenous Communities," The Belfer Center, Harvard Kennedy School, Dec. 10, 2020, video, https://www.belfercenter.org/event/living-uranium-impact-uranium-mining-indigenous-communities.

dam burst. In areas downstream of the spill, she said, people "actually waded through the water to get to their livestock across the arroyo." Since then, she's seen the landscape continue to change as new mines have been excavated and old ones abandoned. In one of the childhood pictures Keyanna showed, she and her cousins play in front of a towering pile of waste rock.

Jeff Gaco, Second Lieutenant Governor of the Laguna Pueblo, spoke at the same panel. The lands of the Laguna Pueblo tribe are adjacent to the Navajo Nation and also bear the legacy of past uranium mining: Gaco recalled dust clouds wafting toward his town from the nearby Jackpile Uranium Mine, which has since been added to the Superfund National Priorities List as a site urgently in need of reclamation.[34] He and other community members, Gaco said, suspected that radioactivity and metal toxicity from the mine was to blame for many of the health disparities faced by the Laguna Pueblo. "We've come across cancers that we've never really had to deal with in the past."

Rates of mortality from cancer are anomalously high in many Indigenous communities, and a 2014 study found that those rates increased among Native Americans from 1990 to 2009, even as they decreased in the white population.[35] That increase is likely the result of a number of factors, including inequitable access to health care and regulated infrastructure, but research has demonstrated links between uranium, arsenic, and cadmium – all present in mine wastes – and various types of cancer.[36] Exposure to heavy metals can also produce a wide array of additional effects, says Johnnye Lewis, the principal investigator with the Navajo Birth Cohort Study. She and her team have found that high levels of uranium in drinking water are associated with an

[34] "Jackpile-Paguate Uranium Mine: Laguna Pueblo, NM," *U.S. EPA,* https://cumulis.epa.gov/supercpad/cursites/csitinfo.cfm?id=0607033, accessed Feb. 2021.
[35] David K. Espey, Melissa A. Jim, Nathaniel Cobb et al., "Leading Causes of Death and All-Cause Mortality in American Indians and Alaska Natives," *American Journal of Public Health*, 104, no. S3 (2014): S303-S11. https://doi.org/10.2105/AJPH.2013.301798.
[36] Lewis, "Mining and Environmental Health Disparities," 133.

increased autoimmune response, in which the body's immune system attacks healthy cells. Those community members who had contact with mine waste also had a much higher likelihood of developing hypertension, diabetes, kidney disease, or some combination of the three.

And as with the Church Rock spill, Lewis says, environmental risk assessments often fail to take into account exposure pathways specific to Indigenous communities. "The science that forms the basis for EPA modeling sometimes is very different from what we see in these communities," she says. In recent years, for instance, her research has suggested that uptake of heavy metals by plants could pose a threat to many tribe members who rely on subsistence agriculture. "That's a major pathway, if you think about agricultural production, you think about animals grazing, you think about people out disturbing soil," she says. "That's a massive potential exposure." Other routes, like inhalation of dust kicked up by horses or the use of plant material for ceremonial purposes, likewise tend to be excluded from risk assessments. And all of these problems, Lewis says, are exacerbated by inadequate infrastructure; many tribal communities, for instance, lack access to clean drinking water. Even on tribal land that has a state-regulated water system, Lewis says, water quality is often far lower than elsewhere in the U.S.

While its radioactivity makes uranium a particularly concerning health hazard, the waste from other types of hardrock mines is by no means benign. The minerals dredged up during any mining operation – coal or hardrock – can break down when they are exposed to oxygen and water, a process that produces sulfuric acid and lowers the pH of nearby waterways. As the acidic water moves over the landscape, it pulls heavy metals, including lead, cadmium, and arsenic, from surrounding rocks.[37] When storage facilities containing waste rock and

[37] Ata Akcil and Soner Koldas, "Acid Mine Drainage (AMD): Causes, Treatment, and Case Studies," *Journal of Cleaner Production,* 14, no. 12 (2006): 1139-1145. https://doi.org/10.1016/j.jclepro.2004.09.006.

contaminated water fail – as they did at Church Rock in 1979 and again in Colorado three and a half decades later – the results can be catastrophic.

In August of 2015, during an investigation of the abandoned Gold King Mine in Silverton, Colorado, water began to leak from a wall fracture after an EPA inspector dislodged a plug. Within hours, three million gallons of water and waste had surged into the Animas River, turning it a muddy orange.[38] A number of watercourses were contaminated, including several on the Navajo Nation. Karletta Chief, a hydrologist at the University of Arizona who is herself Diné, led a team of researchers who monitored water quality after the spill and documented heavy metal exposures faced by Diné communities. She worked with Indigenous families directly and discussed with them the risks the spill might pose. "It's really important to involve communities – to be transparent, to be communicative, to share data, to have the community's input every step of the way." Otherwise, she says, "It can get very contentious very fast and can lead to miscommunication and mistrust that may or may not already exist prior to an environmental catastrophe.

In the aftermath of the spill, the Navajo Nation waged a protracted legal battle against the EPA in an effort to secure compensation for the damages.[39] The struggle is characteristic of attempts to draw attention and resources to areas affected by acid mine drainage, which have continued to falter even after researchers documented its environmental effects extensively. "There has been attention, but it hasn't been sustained," says Shuey. "There hasn't been a political will to appropriate the money." Gaco says the same: "We have the ear of the government, but we don't have both ears of the government."

---

[38] "Gold King Mine Release (2015): USGS Water-Quality Data and Activities," *U.S. Geological Survey*, https://www.usgs.gov/mission-areas/water-resources/science/gold-king-mine-release-2015-usgs-water-quality-data-and?qt-science_center_objects=0#qt-science_center_objects, accessed Feb. 2021.
[39] Julie Turkewitz, "Navajo Nation Sues E.P.A. in Poisoning of a Colorado River," *New York Times*, Aug. 16, 2016.

Erin Savage, senior program manager with an environmental advocacy group called Appalachian Voices, agrees. Acid mine drainage in the area where she works, which includes West Virginia, eastern Kentucky, Virginia, and Tennessee, is primarily caused by coal mining instead of hardrock mining, and the region faces a different set of challenges from those faced by the western states. The fleeting attention given to the problem, however, is one similarity. "States like to claim that they're doing enough work early in the process to stop acid mine drainage from ever occurring, but, I mean, we see on the ground that that's just not the case," she says. Some spills, like those that affect major centers of recreation, do make headlines and attract community support. "Many of the places that I work, it's not a big, beautiful canyon. It's little tiny creeks all over the place that nobody sees, maybe people don't use them for fishing." Those small seeps, even though they can ultimately affect entire watersheds, tend to go unnoticed.

Diné communities have also formed advocacy groups and have worked to bring the issue of mine wastes to the government's attention. As with many marginalized groups, however, the environmental risks they face are often left unaddressed, even as heavy metals continue to contaminate Indigenous water and land. Shuey points out that, over the last several years, the federal government has prioritized the cleanup of waste piles on non-Indigenous land. "They left the ones on the Navajo Nation in their places, unlined, on the banks of rivers, and there's contamination as a result. In the other communities, they excavated them and took them to remote disposal sites," he says. "That's the history of environmental justice and systemic racism."

For Diné members like Keyanna, that history is an intensely personal one. Her uncles and her father worked at a uranium mine operated by a now-defunct outfit called Kerr-McGee, and her grandmother worked in the company's offices across the road. "It's over a hundred years and

several generations that we've endured this," she says. And as the start date of a planned EPA cleanup of the waste sites by her home has been postponed again and again, the hazards have accumulated. "We started noticing different things happening to the land, to the livestock, to ourselves." And as the hazards have become more apparent – with little relief in sight – Keyanna says that Diné communities are dwindling as young people leave, aiming to distance themselves from the hazardous waste. Nonetheless, she continues her advocacy work in the hope that the federal government will once and for all take this environmental threat seriously. "We want the land to be restored," she says. "We call that *Hózhó*. It's just a balance between ourselves and the land."

INTRODUCTION

I. Acid mine drainage: Scope, effects, and management

Acid mine drainage (AMD) is one of the most pervasive environmental hazards posed by extractive industry in the United States (U.S. EPA, 1994). Produced during the oxidation of sulfide minerals exposed to air and water, AMD runoff is typically characterized by low pH and elevated concentrations of dissolved sulfate and heavy metals, making it a threat to both ecosystem and human health (e.g., Gray, 1997). Given these risks, AMD has garnered considerable attention; understanding the complex reaction networks that govern these systems is crucial to the development of efficient and effective strategies for their management.

Metal sulfides are abundant in the Earth's crust, and oxidation of these minerals can produce acidic, metal-rich leachates in systems free from immediate anthropogenic influence (Fernández-Remolar et al., 2005; Nordstrom, 2015). With the advent of coal and metal mining, however, this process has accelerated, as ore extraction brings sulfide minerals to the surface in large quantities and exposes them to oxygen and water (Toran, 1987; Akcil and Koldas, 2006; Lottermoser, 2010; Rimstidt and Vaughan, 2014; Lindsay et al. 2015; Skousen et al., 2019). Large piles of waste rock, for instance, generated during mine excavation and rich in metal sulfides, can produce AMD as water percolates through the waste area (Biesecker and George, 1965; Barnes and Romberger, 1968). In addition, processing ores to isolate economically valuable materials like copper or gold leaves behind waste material that is concentrated in sulfide minerals and heavy metals; known as "tailings" and typically stored in ponds and other surface impoundments, this material is of particular concern as a generator of AMD (Lottermoser, 2010).

The most abundant sulfide mineral in the crust, and the dominant contributor to AMD, is pyrite (FeS_2), with other metal sulfides (including pyrrhotite ($Fe_{1-x}S$), sphalerite (ZnS), and

chalcopyrite ($CuFeS_2$)) playing a lesser role (Blodau, 2006). The basic chemistry of pyrite oxidation is described in the following section; the key environmental effects stem from the release of H^+ ions and the increased solubility of heavy metals as the water becomes more acidic. Further, elevated metal loads foster the eventual precipitation of iron (oxy)hydroxides. These effects are mediated by a range of factors; for instance, the ultimate pH of an AMD-affected system depends not only on the amount of metal sulfide available to oxidize, but also on the presence of acid-consuming compounds like carbonates and clays, which can neutralize the acidity generated through pyrite oxidation (Barnes and Romberger, 1968; Nordstrom, 2011). AMD fluids are frequently acidic; the pH of mine waters from Iron Mountain, California, for example, has been recorded as -3.6 (Nordstrom et al., 2000). However, some systems, depending on their host geology, can be near neutral or even alkaline (Toran, 1987; Blodau, 2006).

Of potentially greater concern than the pH of AMD runoff is its heavy metal content. A number of processes contribute to the high concentrations of metals and metalloids, including As, Co, Cu, Pb, Ni, and Zn, in AMD fluids (Cravotta, 2008; Nordstrom, 2011). Pyrite can contain heavy metals as impurities in its crystal structure, which are released upon oxidation; additionally, other metal sulfides like arsenopyrite (FeAsS) and galena (PbS) are frequently present in mine wastes and oxidize alongside pyrite (Blodau, 2006; Rimstidt and Vaughan, 2014). By virtue of its generally low pH, AMD runoff also leaches these metals from surrounding bedrock (Biesecker and George, 1965; Lottermoser, 2010; Punia, 2021). Dissolved metals are often temporarily removed from solution by co-precipitation. For instance, evaporation of water from AMD systems can leave behind melanterite (ferrous sulfate), which then undergoes a series of mineralogical transformations, incorporating trace metals throughout the process (Hammarstrom et al., 2005; Rimstidt and Vaughan, 2014; Buzatu et al., 2016).

Moreover, if the pH of the system is sufficiently high, ferric iron can precipitate as a hydroxysulfate mineral (e.g., jarosite) or as an oxyhydroxide like ferrihydrite or schwertmannite; these minerals are efficient sorbents and also incorporate trace metals (Sánchez España et al., 2005; Park and Kim, 2016). Co-precipitation mitigates the heavy metal content of AMD fluids, but when the host minerals dissolve – as frequently happens with sulfate salts during heavy rains – the sudden release of these trace elements can result in dangerously high concentrations (Rimstidt and Vaughan, 2014).

The products of pyrite oxidation present a host of environmental hazards, influencing ecosystems at every level. Acid sulfate soils, for instance, are more prone to erosion and can affect the quality of nearby water bodies, even if those water bodies do not directly receive AMD runoff (Powell and Martens, 2005; RoyChowdhury et al., 2015). Acidity and heavy metal contamination can kill freshwater species, especially fish, reducing biodiversity and dramatically altering the benthic food web (Gray, 1997; Hogsden and Harding, 2012). Even species that can tolerate the chemical changes may migrate if their food sources are affected or if their habitats are sufficiently reshaped by mineral precipitation (Gray, 1997). Humans, meanwhile, can come into contact with AMD contamination in a number of ways. Drinking or otherwise using AMD-affected water can expose communities to heavy metal toxicity, with the added threat of radiation exposure in the case of uranium mining (Lewis et al., 2017). Heavy metals can also bioaccumulate in food webs, initially taken up by plants, macroinvertebrates, and bottom-feeders, leading to high concentrations in the tissue of the organisms that eat them (Elder, 1988; Cravotta, 2008; Chamorro, 2018).

AMD is widespread in the United States and has been estimated to contaminate over 20,000 kilometers' worth of streams and rivers across the country (U.S. EPA, 1994). Its effects,

however, are unevenly distributed; hard rock mines, for instance, are disproportionately located near Indigenous communities, who bear an inordinate share of the contamination burden generated by well over a century of mining (Lewis et al., 2017; Beckett and Keel, 2019). Toxicity and environmental assessments often neglect to take into account pathways of AMD exposure relevant to Indigenous peoples' day-to-day lives. For instance, many of these communities lack access to reliable water infrastructure or committed government regulation of water quality; because groundwater is susceptible to AMD contamination, the wells that many communities rely on can expose members to dangerously high levels of toxic material even when the water systems of nearby cities have been deemed safe (Brugge et al., 2007; Lewis et al., 2017).

The hazards presented by AMD have made its management a topic of extensive research (e.g., Kleinmann, 1990; Evangelou and Zhang, 1995; Romano et al., 2003; Jacobs et al., 2014; Abinandan et al., 2018; Park et al. 2019). At many sites, sulfide oxidation and AMD generation began decades ago, and the mines have long since been abandoned; tens of thousands of abandoned mines are estimated to produce AMD runoff in the United States (U.S. EPA, 1994). In these cases, contaminated water must be treated as it is being produced, in a process known as "remediation" (Gray, 1997; Akcil and Koldas, 2006). Remediation techniques are divided into two categories, "active" and "passive" (RoyChowdhury et al., 2015). Active remediation involves the continual addition of neutralizing agents like lime, soda ash, or sodium hydroxide (Skousen et al., 2019). Passive systems, on the other hand, do not require regular input of material but are generally less effective; such techniques include limestone drains and channels, alkaline leach beds, and, increasingly, constructed wetlands (Johnson and Hallberg, 2005; Skousen et al., 2017; Pat-Espadas et al., 2018; Skousen et al., 2019). All of these methods serve

to raise the pH of AMD runoff and prompt the co-precipitation of heavy metals with the iron (oxy)hydroxides that will form in the increasingly alkaline conditions. Both, however, require a significant input of resources; even passive systems involve regular maintenance as precipitates encrust surfaces and need to be removed (Skousen et al., 2017). Moreover, due to the self-catalytic nature of pyrite oxidation (see below), the process is incredibly difficult to stop once it has begun (Park et al., 2019); treating the contaminated runoff indefinitely can quickly become prohibitively expensive.

As a result, preventive measures – blocking pyrite oxidation before it starts – are considered ideal (Evangelou and Zhang, 1995; Skousen et al., 2019; Park et al., 2019). A method known as "acid-base accounting" allows mine operators to estimate the acid-generating potential of a given ore body according to its mineralogy (Blodau, 2006; Dold, 2017; Skousen et al., 2019). Overburden removed in the excavation of a mine, as well as the waste generated during mine operation, can then be stored in such a way that oxidation of its constituent sulfide minerals is slowed or prevented. Some of the least resource-intensive methods include soil covers and subaqueous disposal, which serve to prevent significant amounts of oxygen from reaching the waste rock (and therefore reduce the rate of sulfide oxidation), but are not always feasible, particularly in arid regions (Romano et al., 2003; Park et al., 2019).

A category of preventive techniques that has garnered considerable attention is microencapsulation (Evangelou, 2001). In general, microencapsulation works by coating pyrite particles in a material like ferric phosphate (Huang and Evangelou, 1992) or potassium phosphate (Ji et al., 2012), which prevents oxidants from reaching the pyrite surface and thereby passivates it. More recently, however, researchers have turned their attention to carrier-microencapsulation, which specifically targets sulfide minerals (rather than coating all waste

minerals indiscriminately) and so reduces the amount of passivating material required; these strategies typically involve the mixing of mine wastes with metalloid-organic complexes that decompose only when in contact with sulfide minerals, producing metalloid-oxyhydroxide coatings on the mineral surface and limiting oxidation (Satur et al., 2007; Thakur Jha et al., 2012; Park et al., 2018; Li et al., 2019).

Microencapsulation techniques, and carrier-microencapsulation techniques in particular, typically involve more than the simple addition of a passivating agent to a waste deposit. Instead, these methods tend to require the addition of one or more precursor compounds, which will then undergo a series of interactions on and near the pyrite surface, ultimately resulting in a passivating layer (Park et al., 2019). Therefore, successful deployment of these techniques requires an intimate understanding of pyrite oxidation chemistry. Knowledge of the mechanistic steps involved allows researchers to target individual parts of the process and therefore develop more specific and efficient prevention strategies. This work aims to refine our mechanistic understanding of pyrite oxidation and thereby facilitate the development of effective techniques to address this pressing environmental concern. In the following section, I outline the state of knowledge regarding the mechanism of pyrite oxidation, as well as the lingering questions that this research intends to address.

II. Basic pyrite oxidation chemistry

The stoichiometry of pyrite oxidation by its two principal oxidants, O_2 and ferric iron (Fe^{3+}), has been known for several decades (Garrels and Thompson, 1960; Singer and Stumm, 1970; Lowson, 1982). In aqueous solutions, pyrite is oxidized by molecular oxygen according to the following equation:

$$FeS_{2(s)} + 7/2O_2 + H_2O \rightarrow Fe^{2+} + 2SO_4^{2-} + 2H^+ \textbf{ (Eq. 1).}$$

In the presence of molecular oxygen, the ferrous iron (Fe^{2+}) produced is oxidized to Fe^{3+} through **Eq. 2** and, if the pH of the system is sufficiently high, will precipitate as iron hydroxide according to **Eq. 3**:

$$4Fe^{2+} + O_2 + 4H^+ \rightarrow 4Fe^{3+} + 2H_2O \textbf{ (Eq. 2).}$$

$$Fe^{3+} + 3H_2O \rightarrow Fe(OH)_{3(s)} + 3H^+ \textbf{ (Eq. 3).}$$

In neutral- to high-pH systems that favor iron hydroxide precipitation (for instance, abandoned mines whose host geology contains significant amounts of carbonate minerals or clays), these three equations can be combined as follows:

$$FeS_{2(s)} + 15/4O_2 + 7/2H_2O \rightarrow Fe(OH)_{3(s)} + 2SO_4^{2-} + 4H^+ \textbf{ (Eq. 4).}$$

In low-pH systems where Fe^{3+} remains in solution, it can act as a second oxidant for pyrite as follows:

$$FeS_{2(s)} + 14Fe^{3+} + 8H_2O \rightarrow 15Fe^{3+} + 2SO_4^{2-} + 16H^+ \textbf{ (Eq. 5).}$$

As these equations demonstrate, the reactions involved in pyrite oxidation are not independent of one another. Most prominently, coupling **Eq. 2** and **Eq. 5** forms a self-catalytic cycle wherein FeS_2 oxidation produces Fe^{2+}, which is oxidized to Fe^{3+} and then itself oxidizes FeS_2 to produce more Fe^{2+}; this is a key reason why AMD prevention is preferable to post-formation treatment, which could continue almost indefinitely (Singer and Stumm, 1970). While Singer and Stumm (1970) demonstrated that the rate of abiotic oxidation of Fe^{2+} to Fe^{3+} is very low beneath about pH 4, potentially slowing this cycle, microbial oxidation of Fe^{2+} is rapid in that pH range (Williamson et al., 2006). Microbial communities consisting of multiple taxa of acid-tolerant iron- and sulfur-oxidizing bacteria and archaea have been documented in AMD

systems, accelerating these reactions and facilitating runoff formation (Baker and Banfield, 2003; Méndez-García et al., 2015; Nordstrom et al., 2015).

Alongside microbial mediation, several other environmental factors influence rates of pyrite oxidation. Principal among them are oxidant and water availability; exposed pyrite surface area (a function of grain size, coating, and surface geometry (e.g., Fornasiero et al., 1992; Hollings et al., 2000; Dettrick et al., 2019); temperature (e.g., Hollings et al., 2000); and pH (McKibben and Barnes, 1986; Williamson and Rimstidt, 1994; Akcil and Koldas, 2006; Johnson et al., 2019)). Multiple surface-area-specific rate laws have been formulated for the oxidation of pyrite by O_2 and Fe^{3+} (e.g., Smith and Shumate, 1970; McKibben and Barnes, 1986; Moses et al., 1987; Holmes and Crundwell, 2000; Gartman and Luther, 2014) though Johnson et al. (2019) cite the law presented by Williamson and Rimstidt (1994) as the most widely used in the case of O_2:

$$r_{pyrite} = 10^{-8.19(\pm 0.10)}[O_2]^{0.50(\pm 0.04)}[H^+]^{-0.11(\pm 0.01)} \textbf{ (Eq. 6).}$$

where r is the rate of pyrite oxidation in mol m^{-2} s^{-1} and concentrations are in mol/L. Johnson et al. (2019) themselves found a similar relationship, with a slightly more pronounced dependence on pH:

$$r_{pyrite} = 10^{-8.83(\pm 0.27)}[O_2]^{0.50(\pm 0.04)}[H^+]^{-0.25(\pm 0.02)} \textbf{ (Eq. 7).}$$

Similarly, several authors have calculated rate laws for the oxidation of pyrite by Fe^{3+} (Garrels and Thompson, 1960; Moses et al., 1970; Smith and Shumate, 1970; Wiersma and Rimstidt, 1984; McKibben and Barnes, 1986; Rimstidt and Newcomb, 1993; Williamson and Rimstidt, 1994; Holmes and Crundwell, 2000). The rate law presented by Williamson and Rimstidt (1994) under anoxic conditions is as follows:

$$r_{pyrite} = \frac{10^{-8.58(\pm 0.15)}[Fe^{3+}]^{0.3(\pm 0.02)}}{[H^+]^{0.32(\pm 0.04)}[Fe^{2+}]^{0.47(\pm 0.03)}} \textbf{ (Eq. 8).}$$

As understanding of pyrite oxidation kinetics has grown, studies have increasingly focused on the mechanism involved, the complexity of which has made it difficult to decipher. Each elementary step in an oxidation-reduction reaction tends to involve the transfer of only one electron (Basolo and Pearson, 1967), meaning that pyrite oxidation – in which sulfur transitions from the -I to the +VI oxidation state – could involve up to seven elementary steps (Rimstidt and Vaughan, 2003). While it has long been clear that pyrite oxidation involves the adsorption of an oxidant to the pyrite surface (Goldhaber, 1983; Nicholson et al., 1988; Johnson et al., 2019), pyrite is a semiconductor (Biegler and Swift, 1979), meaning that electrons can pass through the material, and all seven elementary steps need not occur at a single site on the pyrite surface (Rimstidt and Vaughan, 2003).

The mechanism presented by Rimstidt and Vaughan (2003), generally known as the "semiconductor model," is central to our understanding of pyrite oxidation. In this framework, oxidation is divided into three steps: a cathodic reaction at an Fe^{2+} site on the pyrite surface; electron transport within the mineral; and an anodic reaction at a sulfur site. Briefly, this model holds that Fe^{2+} on the surface releases an electron to either O_2 or Fe^{3+} and a "replacement" electron then transfers from the anodic site to the cathodic site to reduce the iron back to Fe^{2+}; this gives the sulfur at the anodic site a temporary positive charge and makes it vulnerable to nucleophilic attack by water. According to this version of the model, sulfur is entirely oxidized to sulfate while it is still attached to the pyrite surface; that is, the authors stress that compounds containing sulfur in an intermediate oxidation state (such as thiosulfate, $S_2O_3^{2-}$ or sulfite, SO_3^{2-}) are unlikely to be released into solution.

This model, while seminal, has been continually refined in the years following its proposal. Schoonen et al. (2010), for instance, have suggested that the cathodic reaction is likely

far more complicated than the simple adsorption of an oxidant species and the transfer of an electron, demonstrating the role of hydrogen peroxide as an intermediate. The present work, however, focuses on the reactions taking place at the anodic site. Multiple previous studies call into question the notion that nucleophilic attack by water at the anodic site proceeds all the way to sulfate before releasing a sulfoxyanion into solution. The oxygen isotopic composition of the sulfate produced during pyrite oxidation has proven to be a powerful tool in the investigation of this question. If a given sulfur atom were oxidized completely to sulfate before detaching from the pyrite surface, all four oxygen atoms in that sulfate ion would necessarily have come from successive nucleophilic attacks by water. In that case, the oxygen isotopic composition of the sulfate produced would reflect the oxygen isotopic composition of the ambient water and the oxygen isotope fractionation factor between sulfate and water (Van Stempvoort and Krouse, 1994). (More specific definitions of the measures of oxygen isotopic composition are provided below.) Instead, several studies using $\delta^{18}O$ labeling have suggested that between 2% and 29% of the oxygen in sulfate produced during oxic, abiotic pyrite oxidation may come from O_2 (Taylor et al., 1984; Balci et al., 2007; Tichomirowa and Junghans, 2009; Kohl and Bao, 2011).

These isotopic observations could still be consistent with a model of oxidation in which nucleophilic attack by water oxidizes sulfur at the anodic site all the way to sulfate. Current understandings of the cathodic reaction at the Fe^{2+} site suggest that adsorbed O_2 may react with H^+ to form H_2O_2 as an intermediate, which then reacts to form water (Schoonen et al., 2010). If that water then oxidizes a sulfur atom on the pyrite surface, it could impart the oxygen isotopic signature originally present in O_2 to the product sulfate. Because ambient water is presumably far in excess of the other oxygen sources, however, isotopically distinct water produced at the cathodic site would likely have a negligible impact on the isotopic composition of the H_2O pool.

Instead, it has been assumed that the O_2 isotopic signal in product sulfate is the result of direct oxidation of an intermediate sulfoxyanion by O_2 itself (Kohl and Bao, 2011).

Indeed, previous work has demonstrated that sulfoxyanions like sulfite and thiosulfate are in fact present during pyrite oxidation under certain conditions, if only in minor concentrations. Goldhaber et al. (1983) detected various sulfoxyanions over the pH range 6-9 and documented a clear pH influence over relative concentrations; thiosulfate and, to a lesser extent, sulfite, dominated at higher pH, while sulfate and tetrathionate ($S_4O_6^{2-}$) increased in relative abundance with decreasing pH. Moses et al. (1987) also found that thiosulfate and the polythionates ($S_nO_6^{2-}$) were present in significant amounts above pH 3.9. Rimstidt and Vaughan (2003) acknowledge these findings but point to studies of the sulfur isotopic composition of product sulfate (e.g., Toran and Harris, 1989) as evidence against any significant role for sulfoxyanion intermediates. They also cite work by Williamson and Rimstidt (1993) that suggests thiosulfate is unstable in the presence of Fe^{3+}, but Kohl and Bao (2011) find significant concentrations of thiosulfate (and sulfite) during pyrite oxidation at high pH, even in solutions with Fe^{3+} added.

The variation in these findings suggests that further investigation is required to fully understand the role of sulfoxyanion intermediates during pyrite oxidation and, more specifically, the influence of these intermediates on the final oxygen isotopic composition of sulfate produced in the process. This work will attempt to elucidate that influence in three related ways:

1. By monitoring the production of intermediate sulfoxyanions during pyrite oxidation across a range of pH, oxidant, and mineralogic conditions;
2. By determining the equilibrium oxygen isotope fractionation factors between sulfite and water (cf. Wankel et al., 2014) and thiosulfate and water under a variety of conditions in

order to better understand the controls on the oxygen isotopic composition of the sulfate produced during pyrite oxidation;

3. By applying the isotope systematics described above to a mining-affected environment, in order to constrain the possible pathways by which sulfate is formed in AMD systems.

By further elucidating the role of intermediate sulfoxyanions in the pyrite oxidation process, this work aims to refine our understanding of the various mechanisms by which AMD products form, hopefully facilitating the development of targeted strategies to prevent it and to mitigate its environmental effects.

METHODS

We conducted a series of experiments to investigate the role of the aqueous sulfoxyanions thiosulfate ($S_2O_3^{2-}$), sulfite (SO_3^{2-}), and sulfate (SO_4^{2-}) in the pyrite oxidation process. In order to monitor the concentrations of these species as pyrite oxidizes under a variety of conditions, we performed three separate batch experiments that differed in pH, oxidant availability, and pyrite grain size. We also conducted a range of incubation experiments involving aqueous sulfite and thiosulfate, to determine the equilibrium oxygen isotope fractionation factors between each of these sulfoxyanions and water. Ultimately, we applied these results to a natural environment by measuring the oxygen isotopic composition of sulfate present in water samples from a former gold mine and using the data in concert to constrain pyrite oxidation pathways in an AMD system.

I. Pyrite oxidation batch experiments

All experiments were conducted with Ward's Science pure cubic pyrite, ground in a ShatterBox ring and puck mill and sieved to obtain the appropriate grain size fraction. Pyrite grains between 63 and 250 μm in diameter were used for the first batch because a similar size fraction has been found to characterize sandstone uranium deposits, suggesting that it is representative of the pyrite that generates AMD in regions where uranium is mined (McKibben and Barnes, 1986). The second batch was conducted with pyrite grains between 20 and 45 μm in diameter, to monitor the effects of mineral surface area on sulfoxyanion formation.

Both size fractions were cleaned according to the procedure outlined by Moses et al. (1987, denoted as "Method 3" in that manuscript). Pyrite was submerged in 6 M hydrochloric acid and allowed to sit in a hot-water bath for fifteen minutes before decanting. It was then rinsed

three more times with hot hydrochloric acid, once with Milli-Q water, and twice with acetone. This cleaning procedure removes fines, organics, and surface oxide coatings that may affect oxidation rate (Rosso and Vaughan, 2006; Murphy and Strongin, 2009). After drying overnight at 70°C, pyrite was stored in a helium-flushed septum bottle to prevent oxidation. To identify the specific surface area of the pyrite used, a sample of each grain size fraction stored in a helium-flushed bottle was characterized via N_2-BET analysis. The specific surface area of the 20-45 μm size fraction (after cleaning) was measured as 2.295 m^2/g. The surface area of the 63-250 μm size fraction was below the detection limit of the instrument. Approximation as a collection of spherical grains produces an unreliable estimate of surface area; for instance, calculating the specific surface area of the smaller grain size fraction this way yields an estimate ~60 times lower than the measured value. Therefore, measurements requiring normalization to surface area are not reported for the larger grain size fraction.

Both experiments were conducted using glassware rinsed in nitric acid to ensure the absence of microbes and remove any trace metals. In each batch, pyrite was allowed to oxidize at three pH values, in solutions prepared using three 0.02 M buffers: potassium chloride-hydrochloric acid (pH ~2); histidine (pH ~7); and glycine-sodium hydroxide (pH ~10). These buffers were chosen because they involve no anions that will precipitate appreciably with Ba^{2+}, at the concentrations used, when barium chloride is added to the solution; this was not relevant for these batch experiments, but it was a necessary consideration for the sulfoxyanion equilibrium experiments (see next section), and the same buffers were used in both sets of experiments for consistency. A list of all batch experiments and their respective conditions is provided in **Table 1**.

Experiment No.	Oxidant	Grain Diameter (μm)	pH	Duration (d)
1	O_2	63-250	2	80
2	O_2	63-250	7	80
3	O_2	63-250	10	80
4	O_2	20-45	2	21
5	O_2	20-45	7	21
6	O_2	20-45	10	21
7	Fe^{3+}	20-45	2	22
8	Fe^{3+}	20-45	7	22
9	Fe^{3+}	20-45	10	22

Table 1. Summary of pyrite oxidation batch experiments performed. Fe^{3+} was added as solid hematite (Fe_2O_3). Target pH values for each experiment are recorded; the actual pH value of a replicate never differed from the target pH value by more than 0.05 pH units.

For the larger size fraction experiments (Experiments 1-3 in **Table 1**), 1 g of pyrite (63 to 250 μm) was added to 300 mL of buffered solution in a 500-mL septum bottle, capped, and crimped with a septum stopper to prevent further contact with the atmosphere after the experiments were initiated. Four replicate experiments were performed at each of the three pH values. These experiments were buffered individually, so the pH values of replicates are not identical, but all are within 0.05 pH units of the target pH. All bottles were covered with aluminum foil to prevent any influence of hydrogen peroxide photolysis, as hydrogen peroxide is a key intermediate in the pyrite oxidation process (Schoonen et al., 2010). Bottles were placed on a room-temperature (~22°C) shaker table at 120 RPM for 80 days before solution samples were taken for analysis.

The second batch involved both oxic and anoxic experiments. The oxic experiments (Experiments 4-6 in **Table 1**) were prepared by adding 1 g of pyrite from the smaller grain size

fraction to 90 mL of buffered solution in a 150-mL septum bottle (an equal solution:headspace ratio to that of the first batch). The bottles were then capped with a septum stopper and crimped. The anoxic experiments (Experiments 7-9 in **Table 1**) contained the same amounts of pyrite and solution but were prepared to ensure that no molecular oxygen remained in the headspace or dissolved in solution when the experiments were initiated. For each experiment, pyrite was added to a 150-mL septum bottle, along with 1 g of synthetic hematite (Fe_2O_3). Hematite was prepared by the addition of anoxic solutions of NaOH and $NaHCO_3$ to a solution of $FeCl_3 \bullet 6H_2O$ in an anaerobic glovebox, according to the method outlined by Galili et al. (2019). After synthesis, the dry powders were examined by XRD; no phase other than hematite was detected. The purpose of the addition of hematite was to introduce an oxidant, in the absence of O_2, that is likely to be found in AMD-affected environments (Tabelin et al., 2017). The bottles were then capped with a septum stopper, crimped, and flushed with helium for two minutes. Each buffer solution was boiled for about two minutes, sparged with helium for twenty minutes to remove dissolved oxygen, and added to the reaction bottles with a helium-flushed needle. All of the experiments in the second batch, oxic and anoxic, were covered with aluminum foil and placed on a room-temperature shaker table at 120 RPM for the duration of the experimental run. Samples were taken from the oxic experiments after 21 days and from the anoxic experiments after 22 days. All measures of reaction progress are normalized to the duration of the experiment.

Sulfoxyanion concentrations in the samples were analyzed on a Metrohm 930 Compact IC Flex ion chromatograph on 0.1 μm filtered samples. Concentrations were quantified from the peak area using a 6-point calibration curve from 1.77 to 56.6 μM (0.142 to 6.35 mg/L; R^2>0.99). Samples were stored under anoxic conditions before analysis and measured in batches of 9 (with a five-hour run time) to prevent oxidation of sulfoxyanion intermediates during analysis. Sulfite

and sulfate peak separation was achieved by adding 2% acetone to a mobile phase of 3.2 mM sodium carbonate/1 mM sodium bicarbonate in Milli-Q water.

II. Sulfoxyanion equilibrium experiments

Equilibrium experiments for both sulfite and thiosulfate were designed according to the procedures outlined by Wankel et al. (2014) for sulfite. Like those authors, we use the term "sulfite" to refer to the group of sulfoxyanion species in which the sulfur atom has an oxidation state of +IV, which includes sulfite *sensu stricto* (SO_3^{2-}); the two isomers of bisulfite (HSO_3^-); the bisulfite dimer ($S_2O_5^{2-}$); and aqueous sulfur dioxide ($SO_{2(aq)}$). Similarly, we designate as "thiosulfate" all sulfoxyanions containing one sulfur atom in the -I oxidation state and one in the +V oxidation state; this group includes thiosulfate *sensu stricto* ($S_2O_3^{2-}$) and the two protonated isomers ($HS_2O_3^-$). Speciation of sulfoxyanion species is treated in greater detail in the Discussion section.

For each individual sulfite and the thiosulfate experiment, 1 mmol of the appropriate anhydrous sodium salt (Na_2SO_3 or $Na_2S_2O_3$) was placed in a nitric acid-washed culture tube, which was then closed with a septum stopper, crimped, and flushed with helium for two minutes. Each of the three buffered solutions (pH ~2, ~7, and ~10, detailed above) was boiled for two minutes and sparged with helium for twenty minutes. 10 mL of buffered solution was then added to each culture tube with a helium-flushed needle, yielding 0.1 M anoxic solutions of Na_2SO_3 or $Na_2S_2O_3^{2-}$. All buffered solutions were prepared using the same batch of Milli-Q water to ensure that the oxygen isotopic composition of the water was the same for all experiments ($\delta^{18}O$ = -6.45 ± 0.03‰, measured using Picarro cavity ring-down spectroscopy and bracketed to SMOW and

SLAP). Once buffered solution was added, each tube was shaken vigorously and stored at the appropriate temperature for the experimental run.

One set of sulfite experiments was conducted at room temperature (approximately 22°C), with three replicates performed at each pH value. Thiosulfate experiments were conducted at room temperature, 4°C, and 93°C, also with pH-buffered tubes in triplicate. All tubes showed complete and rapid dissolution of their respective salts except those at room temperature and 4°C containing Na_2SO_3 at pH 2, in which the salt gradually and incompletely dissolved. The tubes were left to incubate for ten days, which has been shown by Betts and Voss (1970) to provide ample time for complete oxygen isotopic exchange between sulfite and water. Quenching solutions were prepared in the same way as the sulfoxyanion solutions: barium chloride dihydrate ($BaCl_2 \bullet 2H_2O$) was added to a culture tube that was then sealed and flushed with helium, and helium-sparged buffer solution was added to each tube using a flushed needle to produce 20% weight/weight $BaCl_2 \bullet 2H_2O$ solutions at each pH.

To precipitate the sulfoxyanions as $BaSO_3$ or BaS_2O_3, $BaCl_2 \bullet 2H_2O$ solution at the proper pH and temperature (to prevent re-equilibration of oxygen isotopes) was added to each reaction tube. Enough quenching solution was added to furnish Ba^{2+} five times in excess of SO_3^{2-} or $S_2O_3^{2-}$ to foster quantitative precipitation and therefore avoid the influence of kinetic oxygen isotope fractionation during the precipitation process. Most tubes showed rapid precipitation of the barium salt, with some exceptions. Seven of the 36 reaction tubes (all containing thiosulfate: two at room temperature and pH 2; two at room temperature and pH 7, one at room temperature and pH 10, and two at 93°C and pH 7) did not show appreciable precipitation overnight. When more $BaCl_2 \bullet 2H_2O$ solution was added to these tubes the following day, however, BaS_2O_3 precipitated in all of them. In addition, the three tubes containing $S_2O_3^{2-}$ at 93°C and pH 2

contained yellow solid (presumably elemental sulfur) and smelled strongly of hydrogen sulfide gas during quenching. We suspect that the thiosulfate in these tubes decomposed, as both low pH and high temperature are known to promote the decomposition of thiosulfate into SO_4^{2-} and H_2S; another decomposition pathway yields elemental sulfur, S_8 (Xu and Schoonen, 1995). Precipitates ($BaSO_3$ or BaS_2O_3) were collected from all of the tubes except these three.

Precipitates were rinsed three times with Milli-Q water, after each of which they were centrifuged at 4000 RPM for ten minutes and the supernatant was decanted. Samples were then left in the drying oven at 70°C overnight. The rate of oxygen isotope exchange between $BaSO_3$ and water has been shown to be extremely slow, so any isotopic effects from the interaction between the precipitate and water before complete drying are assumed to be negligible (Wankel et al., 2014). All yields for $BaSO_3$ were over 90% of the expected value, while yields for BaS_2O_3 averaged 73.0% at room temperature, 61.3% at 4°C, and 59.2% at 93°C.

III. Environmental sample sulfate analysis

Samples were originally collected by Osburn et al. (2019) during the establishment of the Deep Mine Microbial Observatory (DeMMO) within the Sanford Underground Research Facility in Lead, South Dakota, USA. The facility is located in what was previously the Homestake Gold Mine, which operated from 1876 to 2001 and discharged substantial amounts of arsenic and other heavy metals into the nearby Cheyenne River (Lewis et al., 2017). Caddey (1991) has characterized the lithology of the site in detail and reports that it is rich in metal sulfides, including pyrite that spans a range of grain sizes. To allow for consistent monitoring of mine fluids, Osburn et al. (2019) modified six previously drilled exploratory boreholes (hereafter denoted as D1 through D6). The six sites differ in depth and lithology and intersect formations

containing varying amounts of pyrite; the particular geology of each borehole site has been documented by Osburn et al. (2019). Those authors also monitored a wide range of geochemical parameters at each of the six sites over the course of two years, providing a detailed record of fluid character over that time (Osburn et al., 2019).

Sulfate was isolated from each of the six borehole samples by passing the fluids through Dowex AG1-X8 anion exchange resin columns in a process modified from Le Gendre et al. (2016). After the samples dripped through the columns, SO_4^{2-} was eluted from the resin by adding 40 mL of 0.4 M hydrochloric acid. 5 mL of 1 M $BaCl_2$ solution was then added to each effluent, in excess of the amount required to quantitatively precipitate as $BaSO_4$ all SO_4^{2-} in the most concentrated sample, according to the SO_4^{2-} concentrations measured by Osburn et al. (2019). Upon precipitation of $BaSO_4$, the effluent solutions were centrifuged at 4000 RPM and the supernatant was decanted. The $BaSO_4$ was then rinsed with 10 mL of Milli-Q water to remove any remaining $BaCl_2$ and the solutions were centrifuged and decanted once more. $BaSO_4$ samples were then dried overnight in an oven at 70°C.

IV. Oxygen isotope analysis of sulfur compounds

The measures of oxygen isotopic composition used here are as follows:

$$R_A = \frac{^{18}O_A}{^{16}O_A} \textbf{ (Eq. 9).}$$

$$\delta^{18}O_A \text{ (per mille)} = \left(\frac{R_A}{R_{std}} - 1\right) \times 1000 \textbf{ (Eq. 10).}$$

$\delta^{18}O$ is measured relative to a standard known as Vienna Standard Mean Ocean Water, or VSMOW. The isotopic compositions of two samples can then be compared:

$$\alpha_{A\text{-}B} = \frac{R_A}{R_B} \textbf{ (Eq. 11).}$$

$$^{18}\varepsilon_{A\text{-}B} = (\alpha_{A\text{-}B} - 1) \times 1000 \textbf{ (Eq. 12).}$$

($^{18}\varepsilon_{A\text{-}B}$ can also be closely approximated by the subtraction of $\delta^{18}O_B$ from $\delta^{18}O_A$.)

The oxygen isotopic compositions of all three precipitated compounds ($BaSO_4$, $BaSO_3$, and BaS_2O_3) were measured on a Thermo Scientific High Temperature Conversion Elemental Analyzer (TC/EA) coupled to a Thermo Scientific Delta V+ continuous-flow gas-source isotope ratio mass spectrometer. Each sample was analyzed in triplicate, alongside the International Atomic Energy Agency (IAEA) standards SO-5 and SO-6 ($\delta^{18}O$ = 12.13 ± 0.33‰ and -11.35 ± 0.31‰, respectively; Brand et al., 2009). Samples were prepared by the combination of approximately 0.2 mg $BaSO_4$ or 0.25 mg $BaSO_3$/BaS_2O_3 (to ensure sufficient oxygen yield) with an equal mass of silver chloride additive in a silver boat before loading into the TC/EA. Average reproducibility of the standards was 0.26‰.

RESULTS

The relative abundances of sulfoxyanions measured at the end of each experimental run are shown in **Fig. 1**, and cross-replicate averages are shown in **Table 2**. Relative abundance was calculated as the concentration of sulfur in a given sulfoxyanion divided by the total concentration of aqueous sulfur; for instance, the relative abundance of sulfur in thiosulfate as a proportion of the full sulfur pool was calculated as: $2[S_2O_3^{2-}]/([SO_4^{2-}] + [SO_3^{2-}] + 2[S_2O_3^{2-}])$. The relative abundances of the three sulfoxyanions exhibited similar qualitative dependencies on pH in the two oxic runs. The sulfoxyanion pool at pH 2 in both surface area conditions was dominated by sulfate, which exhibited an average relative abundance of 98.4% in the low-surface area condition and 99.9% in the high-surface area condition. Accordingly, the intermediate sulfoxyanions (sulfite and thiosulfate) were virtually absent from both oxic runs. Sulfate likewise dominated the sulfoxyanion pool at pH 7 for the high-surface area condition (approximately 78.6% sulfate, 21.1% thiosulfate, 0.4% sulfite), whereas the low-surface area exhibited a more even distribution at pH 7 (34.9% sulfate, 45.2% thiosulfate, 19.9% sulfite). Meanwhile, the relative abundances of the sulfate, thiosulfate, and sulfite at pH 10 differed considerably between the two surface area conditions (11.7%, 30.7%, and 57.6%, respectively, in the low-surface area condition and 35.1%, 40.3%, and 24.6%, respectively, in the high-surface area condition). In both surface area conditions, however, the relative proportion of sulfite shows a clear increase with pH, while the relative proportion of sulfate shows a clear decrease (though sulfate makes up a greater proportion of the sulfoxyanion pool at any given pH in the high-surface area condition than in the low-surface area condition). In both surface area conditions, the combined relative proportion of the aqueous intermediate sulfoxyanions increased with pH, and in both cases intermediate sulfoxyanions dominated at pH 10.

Experimental Condition	pH	Proportion Sulfite (%)	Proportion Thiosulfate (%)	Proportion Sulfate (%)
Oxic, low-surface area	2	1.6	0.0	98.4
	7	19.9	45.2	34.9
	10	57.6	30.7	11.7
Oxic, high-surface area	2	0.1	0.0	99.9
	7	0.4	21.1	78.6
	10	24.6	40.4	35.1
Anoxic, high-surface area	2	0.0	0.0	100.0
	7	0.0	14.5	85.5
	10	0.0	36.5	63.5

Table 2. Average relative abundances of sulfoxyanions across experimental replicates under various oxidant, surface area, and pH conditions. Relative abundance was calculated as $x[S_xO_y^{2-}]/([SO_4^{2-}] + [SO_3^{2-}] + 2[S_2O_3^{2-}])$. Note: one of the three anoxic pH 2 replicates contained no detectable sulfoxyanions.

The anoxic runs (which all had high surface area) exhibited trends in sulfoxyanion distribution similar to those exhibited by the high-surface area oxic runs, with the relative proportion of sulfate decreasing as pH increased (an average of 100.0%, 85.5%, and 63.5% sulfate for pH 2, 7, and 10, respectively) and the relative proportion of thiosulfate increasing with pH (an average of 0.0%, 14.5%, and 36.5% for pH 2, 7, and 10). Sulfite was absent regardless of pH. One replicate of the anoxic experiment at pH 2 did not produce measurable sulfoxyanion concentrations of any species; neither of the other two replicates produced any sulfoxyanion species in excess of 1 μM.

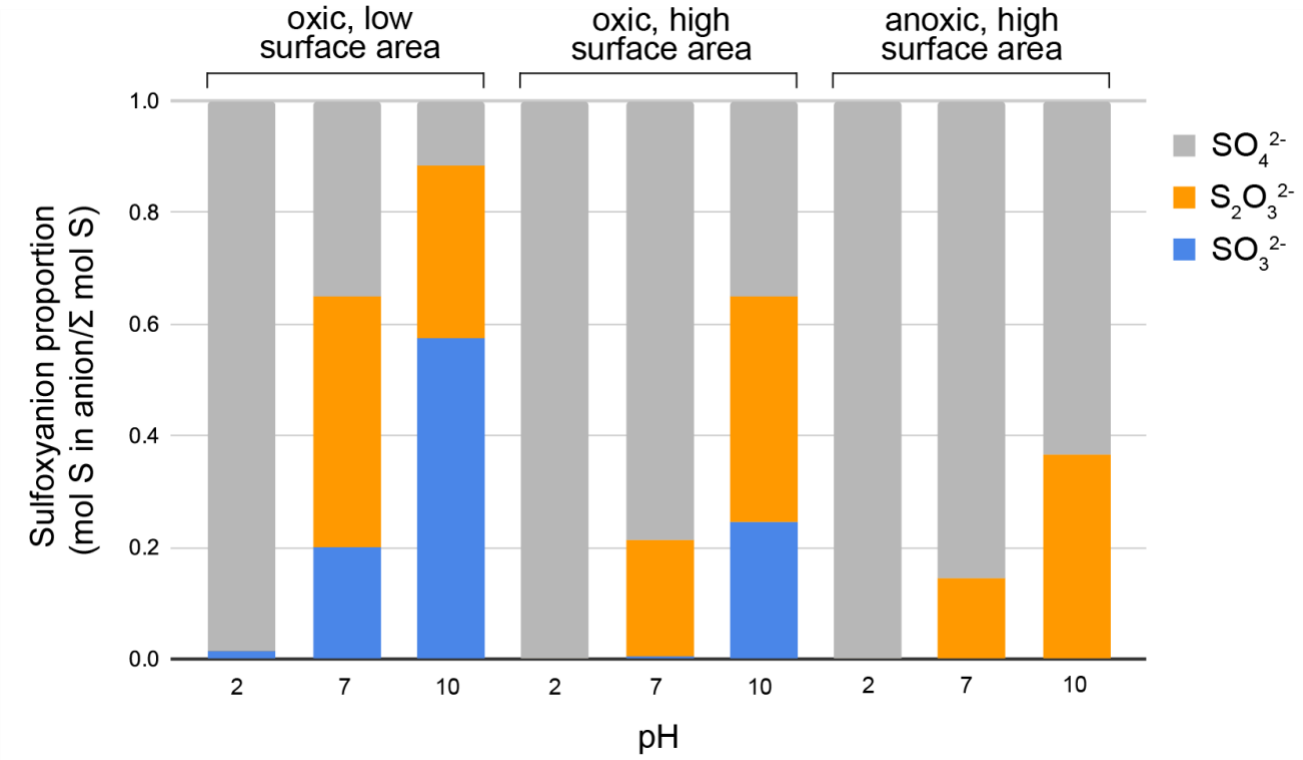

Figure 1. Relative proportions of sulfoxyanions according to pH, oxidant availability, and pyrite surface area. Proportions were calculated as $x[S_xO_y^{2-}]/([SO_4^{2-}] + [SO_3^{2-}] + 2[S_2O_3^{2-}])$.

The mean oxidation state (MOS) of total aqueous sulfur is reported for all experiments in **Fig. 2** as a further visualization of the distribution of sulfoxyanions under each experimental condition. MOS is calculated as follows:

$$MOS = 6f_{SO_4^{2-}} + 4f_{SO_3^{2-}} + 2f_{S_2O_3^{2-}} \textbf{ (Eq. 13).}$$

where f_X represents the fraction of total aqueous sulfur present in species X, as described above. MOS decreased with pH for all conditions, reflecting the varying distributions of aqueous sulfoxyanions. For pH 7 and 10, the anoxic high-surface area condition exhibited the highest MOS, the oxic low-surface area exhibited the lowest MOS, and the oxic high-surface area condition exhibited an intermediate MOS. All conditions exhibited an MOS of 6 at pH 2, reflecting the dominance of sulfate.

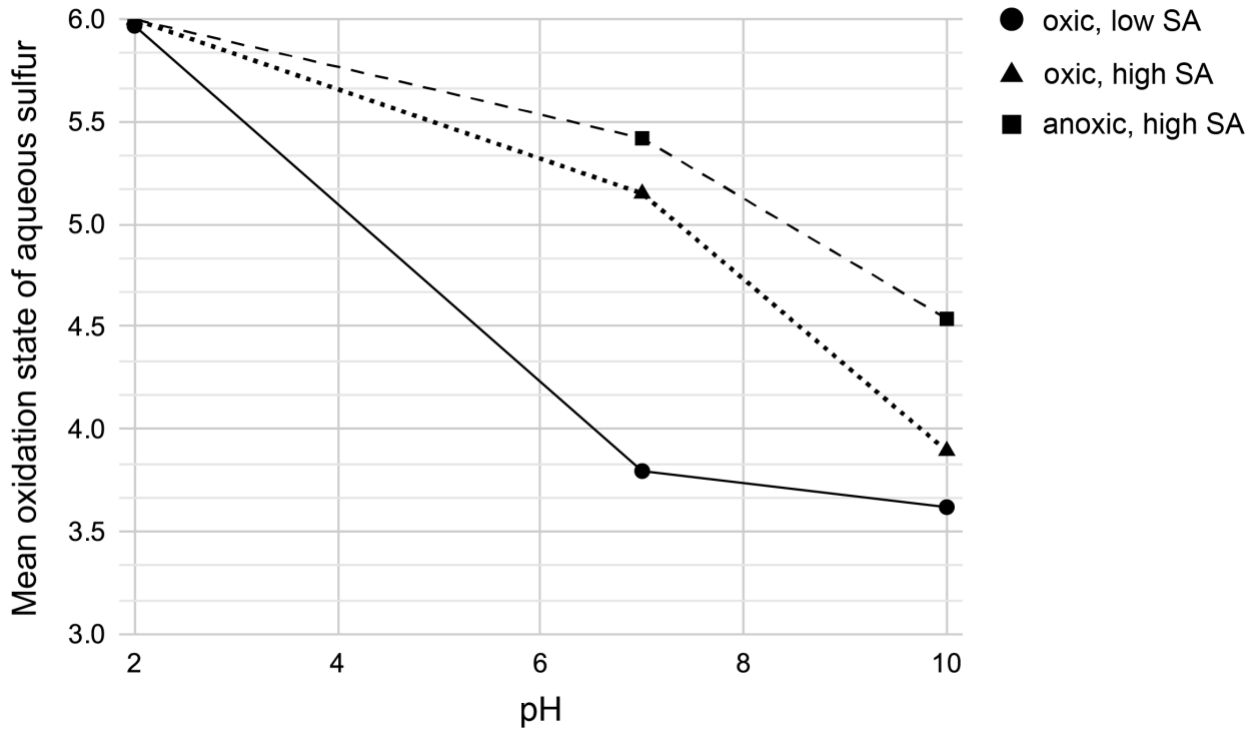

Figure 2. Mean oxidation state (MOS) of aqueous sulfur according to pH and experimental condition. MOS was calculated using **Eq. 13**, above.

The surface area-normalized rates of electron transfer during pyrite oxidation (mmol m^{-2} day^{-1}) are shown in **Fig. 3** for the oxic and anoxic high-surface area conditions. Because the surface area of the larger grain size was not quantifiable via N_2-BET (described above), we do not report normalized rates from those experiments. It is noted, however, that the rate of transfer per day at a given pH (not normalized to surface area) is higher in the high-surface area condition than in the low-surface area condition. We use electrons transferred, rather than another measure of reaction progress, because intermediate sulfoxyanions made up a considerable portion of the overall sulfoxyanion pool in several conditions. If oxidation is complete, the sulfur atom changes from a -I oxidation state in pyrite to a +VI oxidation state in sulfate. In the intermediate sulfoxyanions, thiosulfate and sulfite, sulfur has an oxidation state of

+II and +IV, respectively. (In thiosulfate, this is an average oxidation state, as one sulfur atom has an oxidation state of +V and the other has an oxidation state of -I.) This means that 7 electrons are transferred in the production of sulfate, 5 are transferred in the production of sulfite, and 6 are transferred in the production of thiosulfate. We therefore calculate total electrons transferred, Σe^-, as $7[SO_4^{2-}] + 5[SO_3^{2-}] + 6[S_2O_3^{2-}]$.

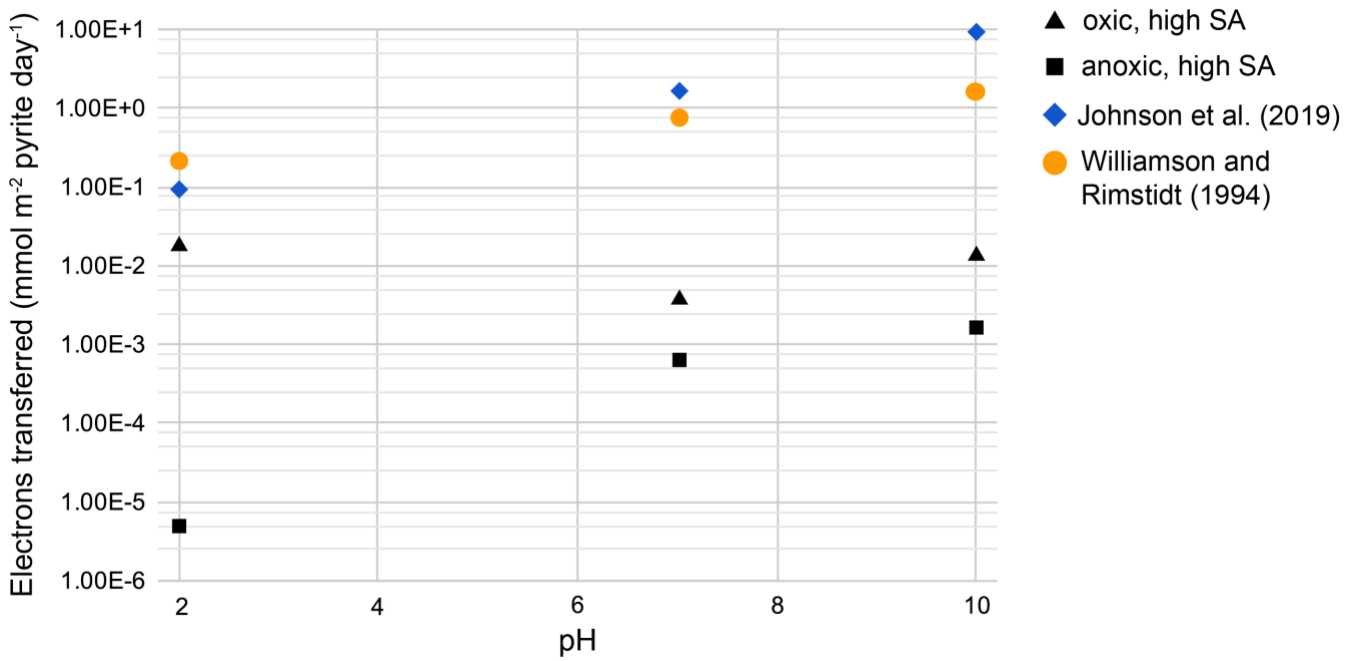

Figure 3. Reaction progress, as represented by rates of electron transfer, according to pH and experimental condition. Rates of electron transfer were calculated by dividing Σe^- by the duration of the experiment. Estimated rates according to the rate laws developed by Johnson et al. (2019) and Williamson and Rimstidt (1994) are included for comparison.

We also include in **Fig. 3** estimates of electron transfer at each pH in oxic conditions according to the rate laws presented by Johnson et al. (2019) and by Williamson and Rimstidt (1994) for the oxidation of pyrite by O_2. These values are calculated by multiplying the rate of "pyrite destruction" given in those studies (mmol m^{-2} day^{-1}) by 14, as the stoichiometry used by those authors to calculate rate laws involves the transfer of 14 electrons.

In the oxic, high-surface area condition, the highest rate of electron transfer occurred at pH 2, the lowest rate at pH 7, and an intermediate rate at pH 10. At a given pH, the rate of electron transfer in these oxic experiments was at least an order of magnitude lower than the rates predicted by both Johnson et al. (2019) and Williamson and Rimstidt (1994). The only exception was pH 2, for which the value calculated in this work and the value predicted by Johnson et al. (2019) differed by less than an order of magnitude. The qualitative dependence of rate on pH under oxic conditions observed here also did not match that predicted by the previous two studies; while both Johnson et al. (2019) and Williamson and Rimstidt (1994) predict an inverse dependence of rate on $[H^+]$, a similar trend did not appear in these data.

The rate of electron transfer under anoxic conditions, by comparison, did increase with pH. Under any given pH condition, the rate of transfer in the anoxic experiments was significantly lower than the rate in the oxic experiments; at pH 2, for instance, the rate of transfer was lower by more than three orders of magnitude in the anoxic condition, as compared to the oxic condition. Comparison with the rate law presented by Williamson and Rimstidt (1994) for the oxidation of pyrite with ferric iron was not possible because of that rate law's dependence on the Fe^{2+} concentration, a value that was not measured in these experiments.

II. Sulfoxyanion equilibrium experiments

The measured oxygen isotope equilibrium fractionation factors $^{18}\varepsilon$ for sulfite-water exchange, across varying pH values at 22°C, are shown in **Fig. 4**. $^{18}\varepsilon_{SO_3\text{-}H_2O}$ was positive at all three pH values and appears to decrease non-linearly with pH. The values range from a cross-replicate average of 9.76‰ at pH 2 to an average of 7.64‰ at pH 10. Also included in **Fig. 4** are the $^{18}\varepsilon_{SO_3\text{-}H_2O}$ values measured by Wankel et al. (2014) at 22°C for pH between 4.5 and 9.8. A

simple linear regression has been performed on the data presented by Wankel et al. (2014), indicating a negative correlation between $^{18}\varepsilon_{SO_3\text{-}H_2O}$ and pH.

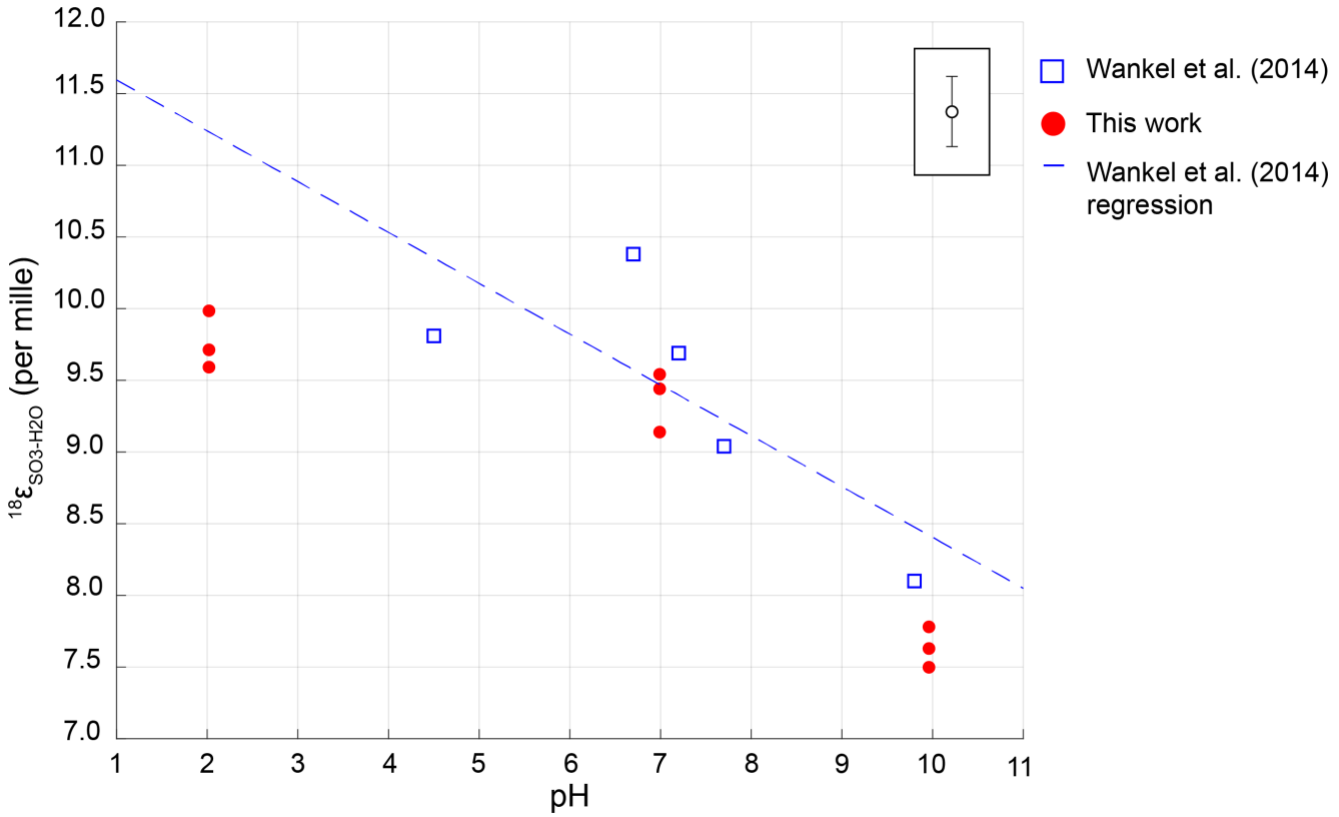

Figure 4. Measured values of $^{18}\varepsilon_{SO_3\text{-}H_2O}$ at 22°C and varying pH. Values measured by Wankel et al. (2014) at 22°C are included for comparison, and a simple linear regression has been performed on those data. The average standard deviation for the standards in this run (0.26‰) is shown in the top right of the plot to indicate the approximate uncertainty above and below each value measured in this work.

For the purposes of further analysis, a Bjerrum plot has been constructed to show the distribution of sulfite species according to pH at the ionic strength of these experimental solutions, 0.3 m (**Fig 5**). The plot includes the species $SO_{2(aq)}$, SO_3^{2-}, and the two isomers of bisulfite, denoted as $(HS)O_3^-$ (tetrahedral) and $(HO)SO_2^-$ (pyramidal) (Eldridge et al., 2016). The first and second acid dissociation constants for the sulfite system, pK_{a1} and pK_{a2} were calculated for an ionic strength

of 0.3 m using the equations presented by Millero et al. (1989). To determine the relative proportions of the two bisulfite species, the isomerization constant presented by Littlejohn et al. (1992) was used. The pH-dependent speciation of the sulfite system was used to visualize the relationship of $^{18}\varepsilon_{SO_3\text{-}H_2O}$ to the proportion of the overall sulfite pool present as bisulfite (**Fig. 5**).

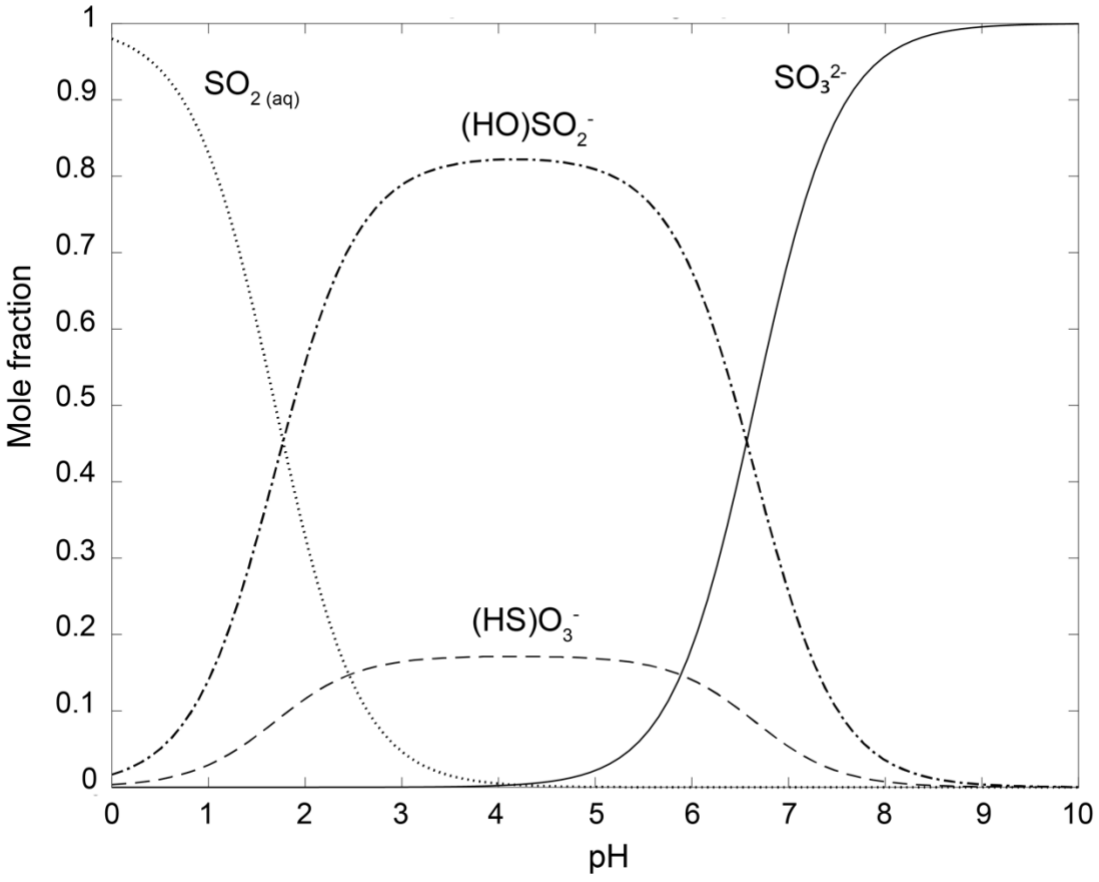

Figure 5. Distribution of sulfite species according to pH for an ionic strength of 0.3. pK_{a1} and pK_{a2} were calculated using the equations presented by Millero et al. (1989). The isomerization constant between bisulfite species is given by Littlejohn et al. (1992).

The $^{18}\varepsilon_{SO_3\text{-}H_2O}$ values measured in this work and by Wankel et al. (2014) were plotted against the logarithm of the bisulfite proportion, and a simple linear regression was performed on the combined datasets (**Fig. 6**).

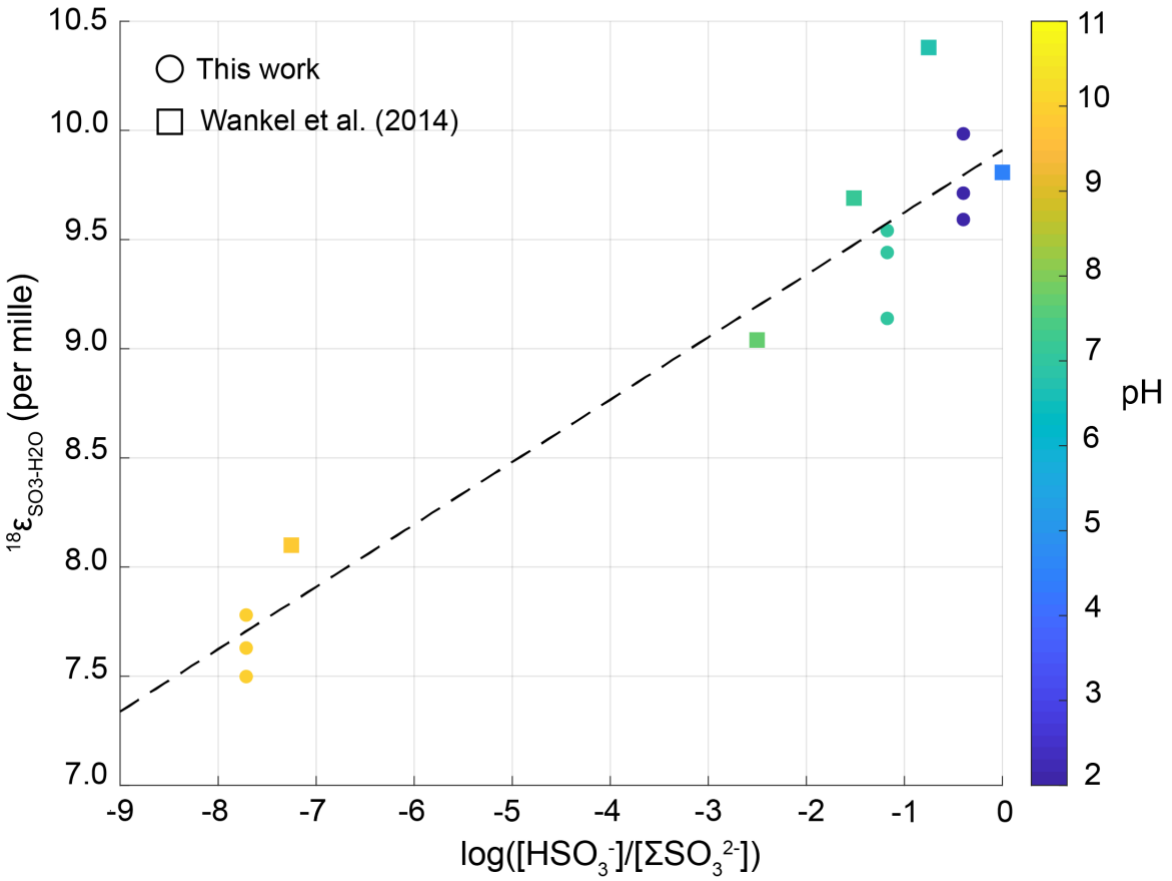

Figure 6. $^{18}\varepsilon_{SO_3\text{-}H_2O}$ according to the logarithm of the proportion of bulk sulfite present as bisulfite, as measured in this work and by Wankel et al. (2014). $[HSO_3^{2-}]$ represents the combined concentrations of both bisulfite isomers.

The measured values of $^{18}\varepsilon$ for thiosulfate-water exchange according to pH at various ambient temperatures and pH values are shown in **Fig. 7**. At 22°C, $^{18}\varepsilon_{S_2O_3\text{-}H_2O}$ was higher by several per mille than $^{18}\varepsilon_{SO_3\text{-}H_2O}$ at a given pH, ranging from a cross-replicate average of 22.11‰ at pH 2 to an average of 14.67‰ at pH 10, with a narrow minimum of 14.25‰ at pH 7. Values of $^{18}\varepsilon_{S_2O_3\text{-}H_2O}$ were similar at any given pH among the three temperature conditions (though, as noted in the Methods section, thiosulfate appeared to decompose at 93°C and pH 2, so

measurements of isotopic composition were not possible for that experimental condition). At 4°C, $^{18}\varepsilon_{S_2O_3\text{-}H_2O}$ ranged from a cross-replicate average of 23.93‰ at pH 2 to averages of 14.43‰ and 14.74‰ at pH 7 and pH 10, respectively. At 93°C, $^{18}\varepsilon_{S_2O_3\text{-}H_2O}$ exhibited cross-replicate averages of 13.02‰ at pH 7 and 14.25‰ at pH 10.

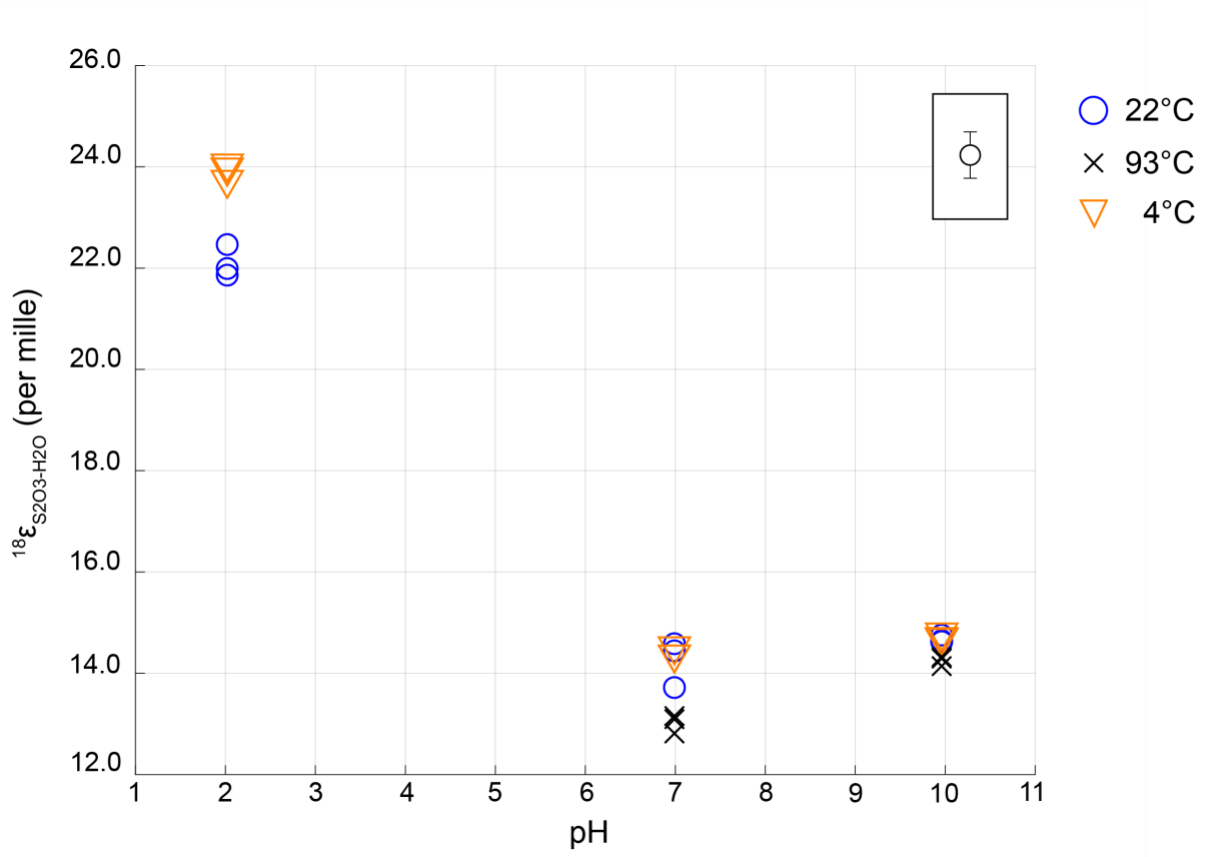

Figure 7. Measured values of $^{18}\varepsilon_{S_2O_3\text{-}H_2O}$ at varying temperature and varying pH. The average standard deviation for the standards in these runs (0.26‰) is shown in the top right of the plot to indicate the approximate uncertainty above and below each measured value. Note: dissolved thiosulfate appeared to have decomposed at 93°C and pH 2, so there are no measurements reported for that condition.

III. Environmental sample sulfate analysis

The oxygen isotopic composition of precipitated sulfate relative to ambient water ($^{18}\varepsilon_{SO_4\text{-}H_2O}$) is reported in **Table 3** for the six DeMMO sites. The average water pH over time, measured by Osburn et al. (2019) is also reported for each site. $^{18}\varepsilon_{SO_4\text{-}H_2O}$ was positive for all sites and spanned a large range of values, from 4.89‰ at site D3 to 24.60‰ at site D6. $^{18}\varepsilon_{SO_4\text{-}H_2O}$ of each sample was plotted against the $[Ca^{2+}]/[Na^{+}]$ and $[SO_4^{2-}]/[Na^{+}]$ of the site's water, also measured by Osburn et al. (2019), in order to assess the potential influence of gypsum ($CaSO_4 \bullet 2H_2O$) or other sulfate-bearing minerals on the isotopic composition of the oxygen in sulfate. There was no clear relationship between these parameters and $^{18}\varepsilon_{SO_4\text{-}H_2O}$, nor was there any apparent relationship between $^{18}\varepsilon_{SO_4\text{-}H_2O}$ and the saturation state of $BaSO_4$ in particular, measured by Osburn et al. (2019).

Site ID	Ambient pH	$^{18}\varepsilon_{SO_4\text{-}H_2O}$ (‰)
D1	7.45	9.69
D2	7.80	8.56
D3	7.09	4.89
D4	8.38	15.88
D5	8.63	16.30
D6	8.48	24.60

Table 3. Oxygen isotopic composition of sulfate precipitated from water samples collected by Osburn et al. (2019) from the Deep Mine Microbial Observatory. $^{18}\varepsilon_{SO_4\text{-}H_2O}$ is calculated by subtracting the $\delta^{18}O$ of the water at each site, measured at intervals over two years by Osburn et al. (2019), from the $\delta^{18}O$ of the sulfate from that site, measured in this work. Reported pH is the average of the pH values measured by Osburn et al. (2019) at each site over the course of two years. As those authors report, the geochemical character of each site did not vary significantly over the period of study.

DISCUSSION

I. Pyrite oxidation batch experiments

A. Controls on aqueous sulfoxyanion distribution

The results of our batch experiments suggest that, under certain conditions, aqueous intermediate sulfoxyanions play a significant role in the pyrite oxidation mechanism. While it is generally accepted that these compounds are present in some form at some point during the oxidation process, multiple questions about their prevalence – including which conditions favor the detachment of these intermediates from the pyrite surface and which conditions permit their accumulation in solution – remain (Xu and Schoonen, 1995; Rimstidt and Vaughan, 2003; Descostes et al., 2004; Descostes et al., 2006; Druschel and Borda, 2006; Kohl and Bao, 2011; Balci, 2017). These experiments allow us to consider the effects of three parameters – pH, oxidant availability, and grain size – on the generation and persistence of intermediate sulfoxyanions in solution.

For the O_2-saturated solutions, the general trends in aqueous sulfoxyanion distribution with respect to pH observed here are in agreement with those documented in the literature. Goldhaber et al. (1983) monitored the distribution of sulfur species over the pH range 6-9 and found that, as a proportion of total sulfur in solution, thiosulfate sulfur and, to a lesser extent, sulfite sulfur, dominated at pH 9; as pH decreased, the dominance of sulfate and tetrathionate increased. Moses et al. (1987) also observed greater accumulation of sulfite and thiosulfate, as well as the polythionates (sulfoxyanions of the form $S_nO_6^{2-}$) at pH 9, as compared to pH 7. These trends have been interpreted (Moses et al., 1987; Rimstidt and Vaughan, 2003; Kohl and Bao, 2011) to reflect a shift in the equilibrium position of the Wackenroder reaction:

$$S_nO_6^{2-} + S_2O_3^{2-} \rightarrow S_{n+1}O_6^{2-} + SO_3^{2-}$$ **(Eq. 14).**

Specifically, because the second acid dissociation constant, pK_{a2}, in the sulfite system is approximately 7, the relative abundance of HSO_3^{2-} compared to SO_3^{2-} will decrease just above pH 7 and increase just below pH 7. Below pH 7, because HSO_3^{2-} is oxidized more easily than SO_3^{2-}, the product SO_3^{2-} (denoting all sulfite species) in **Eq. 14** will be consumed faster, driving the equation to the right and consuming $S_2O_3^{2-}$. In addition, thiosulfate would decompose more readily at lower pH, further depleting its concentration. Above pH 7, **Eq. 14** would be driven to the left, favoring the accumulation of $S_2O_3^{2-}$ (Moses et al., 1987).

This interpretation, while very plausible for the observations by Moses et al. (1987) of high thiosulfate concentrations at pH 9, low thiosulfate concentrations at pH 7, and negligible sulfite at either pH, is complicated by the observations presented in this work. Most notably, because pyrite oxidation serves to lower the pH of the solution in which it occurs, the Wackenroder reaction suggests that pyrite oxidation in a solution initially at pH 7 -- as described above -- should favor the consumption of $S_2O_3^{2-}$ (and, via faster oxidation, SO_3^{2-}) over time. By contrast, our observations show that intermediate sulfoxyanions account for a sizable proportion of all sulfoxyanion species at pH 7, comprising over 60% of the total sulfur pool in the oxic, low-surface area condition and over 20% in the oxic, high-surface area condition (**Fig. 1**). This implies that there is some mechanism apart from the Wackenroder reaction and thiosulfate decomposition at work in the pH-dependent accumulation of aqueous intermediate sulfoxyanions.

In considering this question, it is useful to note that interactions between dissolved species do not provide the only control on sulfoxyanion distribution. As Rimstidt and Vaughan (2003) have pointed out, nucleophilic attack by water on sulfur complexes bound to the pyrite surface can potentially oxidize pyritic sulfur completely to sulfate before the complex is released

into solution. Whether a sulfoxy complex is released into solution before complete oxidation to sulfate (i.e., whether it is released as SO_3^{2-} or $S_2O_3^{2-}$ instead of SO_4^{2-}) is highly dependent upon pH. At high pH, the S-S bond in the S-SO_3 complex ionizes, making it stronger than the Fe-S bond that attaches it to the mineral surface, favoring the release of $S_2O_3^{2-}$ into solution; at low pH, the S-SO_3 complex remains protonated as S-SO_3H, promoting a fourth nucleophilic attack by water and the release of SO_4^{2-} into solution (Rimstidt and Vaughan, 2003). The feasibility of these two paths was further corroborated by spectroscopic analyses indicating the presence of distinct sulfoxyanion complexes on the pyrite surface (Borda et al., 2004). In addition, Druschel and Borda (2006) present a pathway in which the S-S bond breaks, releasing SO_3^{2-} into solution.

While the data presented here are not sufficient to directly distinguish the influences of these two broad controls on sulfoxyanion accumulation – that is, their release from the pyrite surface and their stability in solution – they suggest that an explanation based only on the interactions between aqueous species may be incomplete. A full understanding may require a quantitative model of the rates of release of sulfoxyanion complexes from the pyrite surface. Depending on how those rates vary with pH, for instance, the release of sulfoxyanions from the pyrite surface may be fast enough to compensate for the rightward shift of the Wackenroder reaction, allowing for high concentrations of aqueous sulfoxyanion intermediates even at circumneutral pH. In other words, although our observations are quite consistent with the notion that accumulation of sulfoxyanion intermediates is favored at higher pH (Goldhaber, 1983; Moses et al., 1987; Rimstidt and Vaughan, 2003), our data suggest that sulfoxyanion intermediates may linger in solution across a lower pH range than previously determined; further investigation into the kinetics of sulfoxy complex detachment could help explain this finding.

The effects of grain size and oxidant are potentially more straightforward. At a given pH, aqueous sulfoxyanion intermediates accounted for a smaller proportion of total aqueous sulfur in the high-surface area condition than in the low-surface area condition, and they made up a smaller proportion still in the anoxic condition (**Fig. 1**). This may in part be a result of the factors that control thiosulfate stability in solution. For instance, Xu and Schoonen (1995) have found that the oxidation of thiosulfate to tetrathionate ($S_4O_6^{2-}$) is catalyzed by the mineral surface, which allows for the formation of an intermediate complex between $S_2O_3^{2-}$ and O_2. The rate of this reaction is first order with respect to pyrite surface concentration (m^2/L). The observation that thiosulfate accumulates more readily in the oxic low-surface area condition than in the oxic high-surface area condition (**Fig. 1**) is consistent with this framework.

Oxidized iron (Fe^{3+}) is also known to promote the decomposition of thiosulfate to tetrathionate (Williamson and Rimstidt, 1993; Xu and Schoonen, 1995; Druschel and Borda, 2006). This may help to explain the lower proportion of sulfur present as thiosulfate at a given pH in the anoxic, Fe^{3+}-containing experiments, as compared to the oxic experiments with the same surface area. We were not able to measure the concentration of tetrathionate in these experiments, but its importance as both an oxidation product of thiosulfate and a component of the Wackenroder reaction suggest that it warrants further investigation. Given its role in both heterogeneous and homogeneous reactions that take place during pyrite oxidation, tetrathionate may provide an important link in our understanding of the controls on sulfoxyanion distribution. For now, these experiments indicate that aqueous intermediate sulfoxyanions do play an important role in the pyrite oxidation process, perhaps even under conditions sometimes deemed unfavorable for their accumulation.

B. Rates of aqueous sulfur formation

As these experiments were designed primarily to monitor the presence of aqueous sulfoxyanion intermediates after a period of oxidation, the rate information they provide is limited. As shown in **Fig. 3**, the surface area-normalized rate of electron transfer calculated at the end of the oxic, high-surface area run is approximately an order of magnitude (or more) lower at any given pH than that predicted by the rate laws of Johnson et al. (2019) and Williamson and Rimstidt (1994). This discrepancy is likely explained, at least in part, by differences in transfer rates across the experimental run. Time constraints meant that it was not possible to consistently monitor aqueous sulfur concentrations over the entire course of the run, so the overall rate of electron transfer calculated from these experiments necessarily assumes a constant rate of sulfoxyanion formation. Based on the literature, this is clearly not the case; for instance, Moses et al. (1987) observed a high rate of sulfate formation at the beginning of their experimental runs, followed by a gradual decrease. This is consistent with the rate laws calculated by Johnson et al. (2019) and Williamson and Rimstidt (1994), which present an oxidation rate proportional to $[O_2]^{0.5}$ and inversely proportional to either $[H^+]^{0.25}$ (Johnson et al., 2019) or $[H^+]^{0.11}$ (Williamson and Rimstidt, 1994). Both of those dependencies would serve to decrease the rate of sulfate formation as oxidation progressed, assuming it took place in reaction chambers closed to the atmosphere, as these were. Dissolved O_2 concentrations would decrease as O_2 was consumed by oxidation and pO_2 in the chamber headspace decreased; meanwhile, pyrite oxidation produces H^+ ions. Given that all of these conditions yield a rate of sulfate formation (and therefore electron transfer) that decreases over time, calculating a rate according to a single time point at the end of each experimental run necessarily produces a value that is artificially low. We therefore caution that the rates of oxidation calculated from these results are not reliable as

absolute measures; instead, they are provided for comparison across the experimental conditions monitored in this study.

To that end, it is noted that rates of electron transfer do vary according to pH in these experiments, though the pH dependence observed here for oxic conditions is inconsistent with previous work and should be considered with care. The fact that both oxic experiments present a minimum rate of aqueous sulfur formation at pH 7 is unexpected, considering that the rate laws of Johnson et al. (2019) and Williamson and Rimstidt (1994) predict monotonic variation in oxidation rate across pH. It is plausible that a departure of this sort could be caused by some interaction between the components of the pH buffer and the pyrite, but special care was taken to avoid this. While bicarbonate is known to catalyze pyrite oxidation (Evangelou et al., 1998), preventing the use of a carbonate-bicarbonate buffer for pH 10, none of the buffer compounds used (KCl, HCl, histidine, and glycine) have been shown to produce any rate effect during pyrite oxidation, apart from their influence on $[H^+]$. While the behavior of the oxic experiments differs from that predicted in the literature, however, the anoxic experiments showed the expected qualitative dependence on pH. As shown in **Eq. 8**, the rate of pyrite oxidation by ferric iron in anoxic solutions is inversely proportional to $[H^+]^{0.32}$. Though, as described above, direct numerical comparison to this rate law is not appropriate here, our anoxic experiments do suggest an increasing rate of electron transfer with increasing pH. However, future work that specifically aims to investigate rates of pyrite oxidation in both oxic and anoxic conditions will ideally monitor concentrations of sulfoxyanions at a series of time points.

Nonetheless, these experiments are consistent with previous observations in other ways as well. For instance, the rate of pyrite oxidation is known to depend on mineral surface area (Lowson, 1982; Goldhaber, 1983; Moses et al., 1987; Rimstidt and Vaughan, 2003). Although

the detection limit during N_2-BET measurement did not allow for the quantification of surface area for the larger grain size fraction, it is clear that reaction progress was slower in the oxic experiments with large grains than in the oxic experiments with small grains. In addition, the reaction progress in the anoxic experiments was extremely slow, likely as a result of the very low solubility of hematite in water. Although these experiments were abiotic and are therefore not entirely representative of the natural environment, they are consistent with the finding that soil covers and other means of O_2 deprivation are effective in slowing pyrite oxidation (Romano et al., 2003) even in the presence of a common ferric oxide like hematite.

II. Sulfoxyanion equilibrium experiments

The equilibrium oxygen isotope fractionation factors between sulfite and water presented here for pH 7 and 10 are in good agreement with the values measured by Wankel et al. (2014) at similar pH (**Fig. 4**). Across the pH range used by those authors (4.5 to 9.8) and 22°C, the relation between pH and $^{18}\varepsilon_{SO_3\text{-}H_2O}$ is conceivably linear, and a simple linear regression using those data also fits our measurements at circumneutral and high pH reasonably well. Having extended our experimental conditions down to pH 2, however, we observe a non-linear dependence on pH. Instead, $^{18}\varepsilon_{SO_3\text{-}H_2O}$ appears to vary linearly with $\log([HSO_3^-]/[SO_3^{2-}{}_{tot.}])$ where $[HSO_3^-]$ represents the combined concentrations of both isomers of bisulfite and $[SO_3^{2-}{}_{tot.}]$ represents the concentration of all sulfoxy species in which the sulfur atom has an oxidation state of +IV (**Fig. 6**). A simple linear regression using both these measurements and those presented by Wankel et al. (2014) yields the following relationship:

$$^{18}\varepsilon_{SO_3\text{-}H_2O} = 0.2858 \times \log\left(\frac{[HSO_3^-]}{[SO_3^{2-}tot.]}\right) + 9.9099 \quad \textbf{(Eq. 15).}$$

The dependence of equilibrium oxygen isotope fractionation on the relative abundance of bisulfite in solution is potentially a result of the greater susceptibility of bisulfite (compared to other sulfite species) to nucleophilic attack by water (Moses et al., 1987). Betts and Voss (1970) have shown that the rate of isotopic exchange between sulfite and water decreases from pH ~8.6 to pH 11.0, demonstrating an inverse dependence on the relative proportion of bisulfite; 8.6 is higher than the second acid dissociation constant, pK_{a2} of the sulfite system (**Fig. 5**), meaning that the relative abundance of bisulfite decreases monotonically beyond that point.

However, a faster rate of exchange between bisulfite and water does not necessarily imply that the value of $^{18}\varepsilon$ between bisulfite and water will be different from the value of $^{18}\varepsilon$ between other sulfite species and water. In considering the latter phenomenon, theoretical estimates of the equilibrium oxygen isotope fractionation factors between various sulfite species and water are instructive. The measured $^{18}\varepsilon$ values for the bulk sulfite pool from this work are compared to the theoretical values calculated by Hemingway et al. (in preparation) in **Fig. 8**. As the theoretical values indicate, each species in the sulfite system is expected to exhibit a unique equilibrium oxygen isotope fractionation with water at a given temperature. The bulk $^{18}\varepsilon$ between the sulfite pool and water, therefore, can be expected to reflect the varying distribution of individual sulfite species within that pool; this is consistent with **Fig. 6**, which demonstrates that $^{18}\varepsilon_{SO_3\text{-}H_2O}$ varies with the proportion of sulfite present as HSO_3^-. (Please note that $^{18}\varepsilon_{SO_3\text{-}H_2O}$ is used here to denote the equilibrium oxygen isotopic fractionation factor between the bulk sulfite pool and water; $^{18}\varepsilon_{SO_{3(S)}\text{-}H_2O}$ refers to the theoretical equilibrium oxygen isotopic fractionation factor between sulfite *sensu stricto* and water, represented by the solid line in **Fig. 8**.)

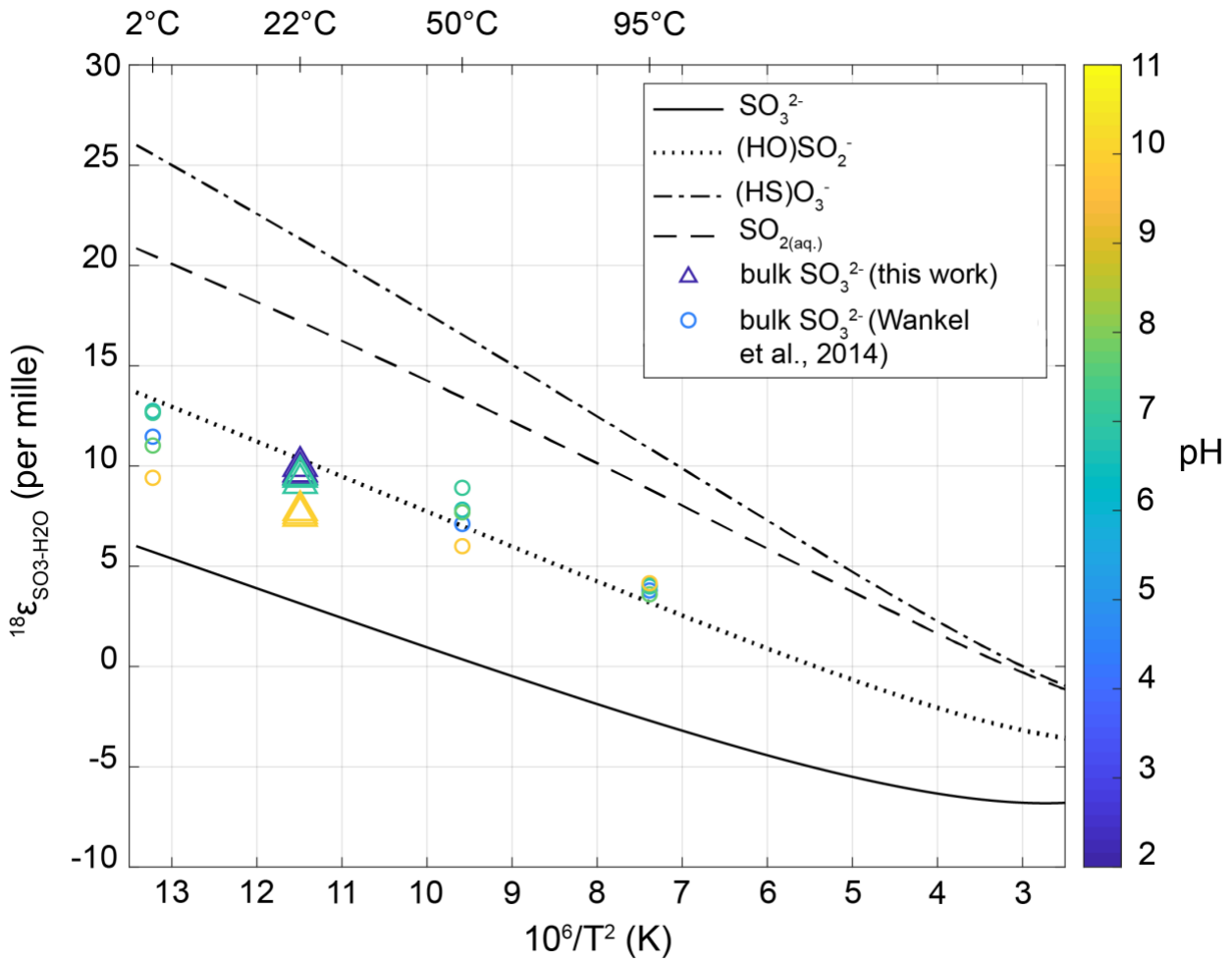

Figure 8. Comparison of measured $^{18}\varepsilon_{SO_3\text{-}H_2O}$ at 22°C and varying pH with theoretical calculations of $^{18}\varepsilon$ between individual sulfite species and water by Hemingway et al. (in preparation). Measurements by Wankel et al. (2014) at 2°C, 50°C, and 95°C are included for comparison and are also color-coded according to pH.

All values measured in this work fall within the range of possible bulk $^{18}\varepsilon_{SO_3\text{-}H_2O}$ as predicted by these theoretical calculations. In addition, the measured values of $^{18}\varepsilon_{SO_3\text{-}H_2O}$ in both this work and the work of Wankel et al. (2014) decrease at the highest experimental pH (10 and 9.8, respectively), falling slightly closer to the predicted value of $^{18}\varepsilon_{SO_{3(S)}\text{-}H_2O}$; this is consistent with the increased relative proportion of sulfite *sensu stricto* at high pH values (**Fig. 5**). As demonstrated by **Fig. 5**, however, the pH range used in this study produces a sulfite pool that

ranges from a relatively even distribution between $SO_{2(aq.)}$ and HSO_3^- at pH 2, through a combination of HSO_3^- and SO_3^{2-} at pH 7, to almost entirely SO_3^{2-} at pH 10. As a result, it is perhaps unexpected that both these measurements of $^{18}\varepsilon_{SO_3\text{-}H_2O}$ and those of Wankel et al. (2014) exhibit a relatively narrow spread compared to the range in values of $^{18}\varepsilon$ predicted for each sulfite species (**Fig. 8**). (In both sets of experiments, measured values of $^{18}\varepsilon_{SO_3\text{-}H_2O}$ cluster closely around the values predicted for $^{18}\varepsilon_{(HO)SO_2\text{-}H_2O}$ at a given temperature, regardless of pH.) The gap between the values predicted for $^{18}\varepsilon_{SO_{3(S)}\text{-}H_2O}$ and the values of $^{18}\varepsilon_{SO_3\text{-}H_2O}$ measured at high pH – under which condition the sulfite pool is composed entirely of sulfite *sensu stricto* – warrants further consideration. For now, this work indicates that $^{18}\varepsilon_{SO_3\text{-}H_2O}$ is sensitive, at least to some extent, to the distribution of sulfite species in solution (**Fig. 6**); in light of the comparison between the measured values of $^{18}\varepsilon_{SO_3\text{-}H_2O}$ and theoretical predictions of $^{18}\varepsilon$ for individual species, the mechanism underlying that sensitivity remains an open question.

The equilibrium oxygen isotope fractionation factors between thiosulfate and water at various temperatures and various pH values are shown in **Fig. 7**. At first glance, thiosulfate appears to reach a different oxygen isotopic equilibrium with water depending on pH, initially suggesting a similar influence of speciation on $^{18}\varepsilon_{S_2O_3\text{-}H_2O}$ as was suggested for $^{18}\varepsilon_{SO_3\text{-}H_2O}$. This possibility is complicated, however, by the fact that the protonated isomers of thiosulfate (denoted as $(HS)SO_3^-$ and $(HO)S_2O_2^-$) are very unstable in solution and have never been detected spectroscopically (Steudel and Steudel, 2009; Eldridge et al., 2016). This makes it unlikely that there could be any significant effect of thiosulfate speciation on $^{18}\varepsilon_{S_2O_3\text{-}H_2O}$. Moreover, as shown in **Fig. 9**, $^{18}\varepsilon_{S_2O_3\text{-}H_2O}$ values at pH 2 are the only ones that closely approach the range predicted by the theoretical model (Hemingway et al., in preparation), with the exception of the values

measured at 93°C (discussed below). Measured values at pH 7 and 10, meanwhile, fall well below the expected range at 4°C and 22°C.

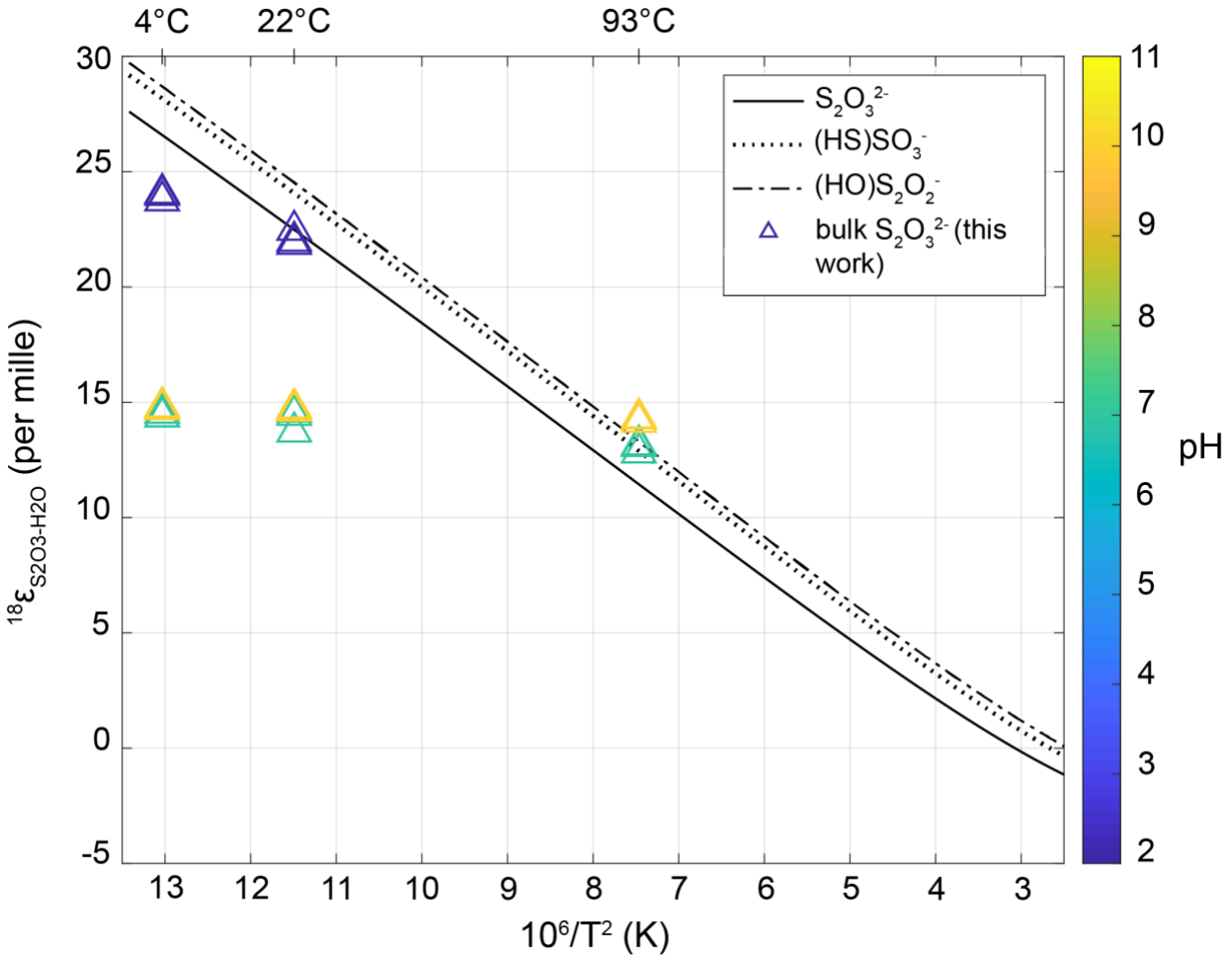

Figure 9. Comparison of measured $^{18}\varepsilon_{S_2O_3\text{-}H_2O}$ at 4°C, 22°C, and 93°C and varying pH with theoretical calculations of $^{18}\varepsilon$ between individual thiosulfate species and water by Hemingway et al. (in preparation). Note: dissolved thiosulfate appeared to have decomposed at 93°C and pH 2, so there are no measurements reported for that condition.

Given the good agreement between the pH 2 data and the predictions, as well as the low likelihood that thiosulfate speciation would exert any appreciable influence on $^{18}\varepsilon_{S_2O_3\text{-}H_2O}$, it seems plausible that thiosulfate did not reach full isotopic equilibrium with water at pH 7 and pH

10. It is noted that **Fig. 9** shows similarity between the $^{18}\varepsilon_{S_2O_3\text{-}H_2O}$ values measured at 93°C and the $^{18}\varepsilon$ values predicted at that temperature, which could indicate that the samples incubated at 93°C had in fact reached isotopic equilibrium with water prior to BaS_2O_3 precipitation. It is reasonable from a kinetic perspective that thiosulfate would reach isotopic equilibrium with water more rapidly at higher temperatures; this is, after all, true of sulfite (Betts and Voss, 1970). It is equally plausible, however, that the measured value simply reflects the starting isotopic composition of the thiosulfate and that this composition coincidentally overlaps with the theoretical predictions for $^{18}\varepsilon$. The similarity between values of $^{18}\varepsilon_{S_2O_3\text{-}H_2O}$ measured for pH 7 and pH 10 at all temperatures suggests that this may be the case. In light of these possibilities, it is unclear whether the values measured at 93°C reflect the true equilibrium isotopic fractionation factor between thiosulfate and water at that temperature.

While the experiments were designed to allow for full equilibration, the kinetics of isotopic exchange between thiosulfate and water are not well constrained, and it is possible that the incubation time was insufficient. In addition, the sluggish precipitation of BaS_2O_3 – especially compared to the precipitation of $BaSO_3$, which was immediate – warrants consideration. The comparatively low yields of BaS_2O_3 (see Results) might suggest that kinetic fractionation occurred during the precipitation of BaS_2O_3, affecting the measured $^{18}\varepsilon_{S_2O_3\text{-}H_2O}$ value. However, there was no significant difference between the percentage yields of BaS_2O_3 at pH 2 and the yields at pH 7 and 10, suggesting that non-quantitative precipitation and the resulting kinetic fractionation were not the cause of the differences in measured $^{18}\varepsilon_{S_2O_3\text{-}H_2O}$ values. It is also worth noting that BaS_2O_3 precipitated rapidly in all of the 4°C experiments (though these yields were also relatively low), another indication that sluggish precipitation of BaS_2O_3 did not produce the gaps in measured $^{18}\varepsilon_{S_2O_3\text{-}H_2O}$ across the pH range.

Given the possibility that the values measured at pH 7 and pH 10 – particularly at 4°C and 22°C – do not reflect an isotopic equilibrium between thiosulfate and water, these values of $^{18}\varepsilon_{S_2O_3\text{-}H_2O}$ are considered to be less reliable than the values measured at pH 2. While it remains possible that these data represent a real dependence of $^{18}\varepsilon_{S_2O_3\text{-}H_2O}$ on pH, the apparent differences may instead be the result of kinetic factors. Future work could begin to address this question by quantifying the rates of the various processes involving thiosulfate, especially its equilibrium oxygen isotopic exchange with water.

III. Environmental sample sulfate analysis

As shown in **Table 3**, the oxygen isotopic composition of sulfate relative to ambient water varies considerably by sample site. While the precise sources of the sulfate in these samples remain poorly constrained, Osburn et al. (2019) did not report the presence of any sulfate-bearing minerals besides barite in the fluid from any of the sites. Given the abundance of pyrite in the host geology of all sites (Caddey et al., 1991; Osburn et al., 2019), we may tentatively assume that the sulfate analyzed in this work was primarily sourced from the oxidation of pyrite and, to a lesser extent, other metal sulfides, in a mine environment.

Assuming that pyrite oxidation is responsible for the majority of the sulfate in these samples, the differences in oxygen isotopic composition between the six sites is striking. **Fig. 10** compares the SO_4^{2-} oxygen isotopic compositions from two sites, D3 and D5, to the equilibrium oxygen isotope fractionation factors for SO_3^{2-} measured in this work. The $^{18}\varepsilon_{SO_3\text{-}H_2O}$ value is calculated for the average pH of each site (7.09 for D3 and 8.63 for D5) using **Eq. 15**.

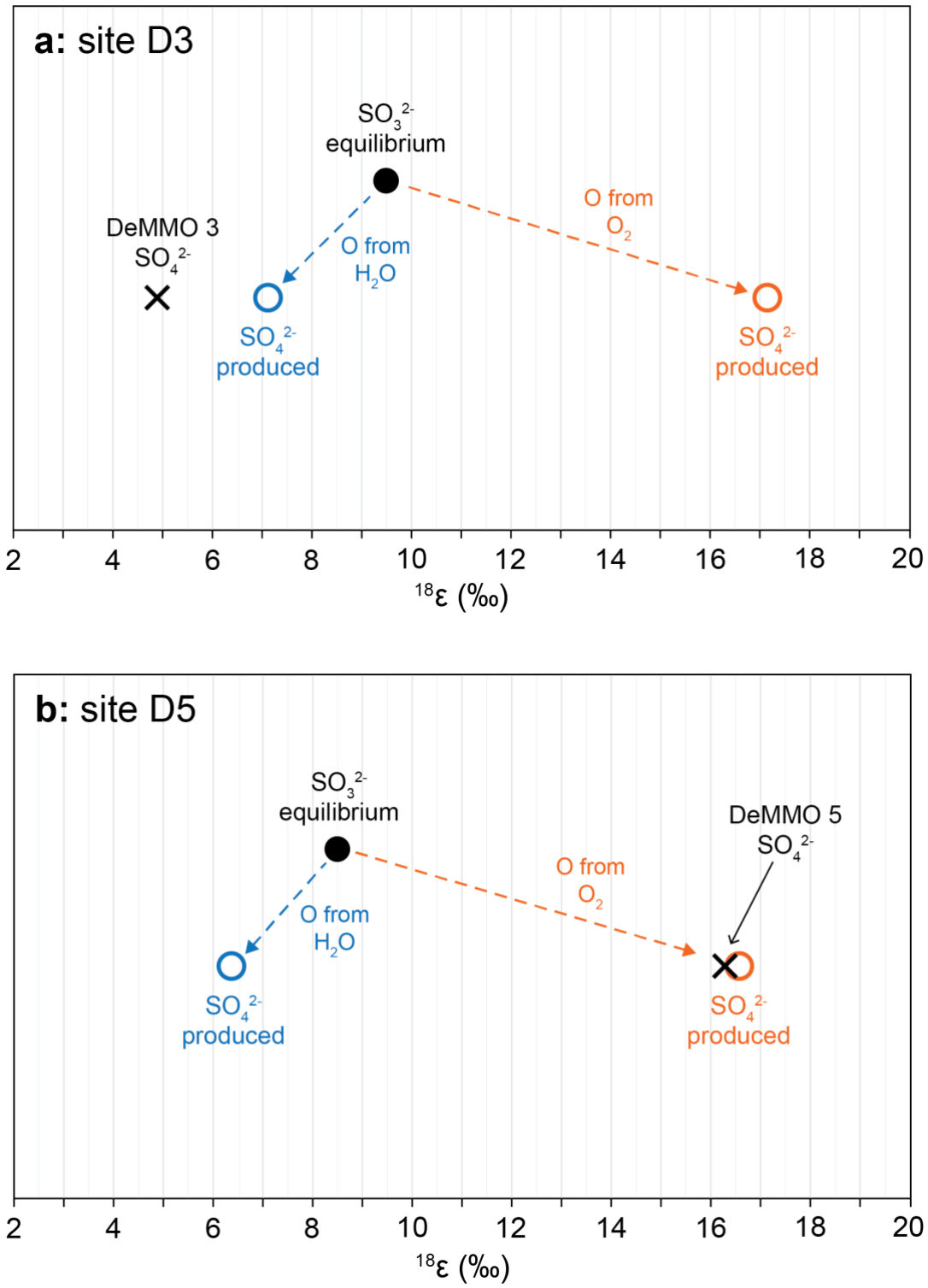

Figure 10. Hypothetical pathways of sulfate formation and expected oxygen isotopic composition at (a) site D3 and (b) site D5. Actual isotopic compositions of DeMMO sulfates are included for comparison. $^{18}\varepsilon$ refers to the equilibrium oxygen isotopic fractionation factor between the relevant sulfoxyanion and water; $^{18}\varepsilon_{SO_3\text{-}H_2O}$ was calculated using the pH of each site, provided by Osburn et al. (2019), and **Eq. 15**.

The equilibrium oxygen isotopic fractionation factor between thiosulfate and water is not included in **Fig. 10** because the values of $^{18}\varepsilon_{S_2O_3\text{-}H_2O}$ calculated in this work for circumneutral pH likely do not reflect full isotopic equilibrium (see above). In addition, current literature suggests that all pathways by which thiosulfate is ultimately oxidized to sulfate must produce sulfite first; sulfite is therefore typically considered to be the direct precursor to sulfate regardless of the exact pathway followed (Kohl and Bao, 2011). The subsequent isotopic equilibration between sulfite and water would then erase the isotopic signature of the thiosulfate precursor in $^{18}\varepsilon$ space. In addition, the equilibrium oxygen isotopic fractionation factor between sulfate and water is not included in **Fig. 10** because the timescale for abiotic equilibration has been determined to be on the order of 10^9 years at temperatures approximating those of the DeMMO sites (Chiba and Sakai, 1985); the oxygen isotopic composition of the environmental sulfate is therefore expected to reflect the isotope systematics of the processes involved in its formation, and not of its equilibration with water.

As shown in **Fig. 10**, at neither site does the $^{18}\varepsilon_{SO_4\text{-}H_2O}$ reflect the isotopic equilibrium between sulfate's precursor, SO_3^{2-}, and water. Instead, the incorporation of a fourth oxygen atom to form sulfate appears to be a crucial step in the determination of the final oxygen isotopic composition of the sulfate. **Fig. 10** depicts two of the primary pathways by which that fourth oxygen atom can be incorporated and which produce two very different oxygen isotopic signatures in the product sulfate. For the purposes of this framework, we assume that the rate of isotopic equilibration between SO_3^{2-} and water is higher than the rate of SO_3^{2-} oxidation by O_2, such that the sulfite-water system can be assumed to reach complete equilibrium and the isotopic signature imparted by reactant SO_3^{2-} is that of pure equilibrium with water. It is important to note, however, that this is not necessarily the case at low pH, under which condition the rate of

oxidation has been shown to exceed the rate of equilibration (Kohl and Bao, 2011; these authors, however, urge caution in the application of their kinetic results). Because the pH conditions of all DeMMO sites are circumneutral, however, it can be assumed that isotopic equilibration between SO_3^{2-} and water is instantaneous.

Even in the case of the simplified representation included here, the influence of sulfate formation pathway on final oxygen isotopic composition is apparent. As suggested by **Fig. 10**, the source of the fourth oxygen is a key control. If sulfite is oxidized by O_2, which is comparatively enriched ($\delta^{18}O = 23.5‰$), the oxygen isotopic composition of product sulfate is driven up. If, by contrast, sulfite receives its fourth oxygen from water ($\delta^{18}O = -16.63‰$ at site D3 and -17.32‰ at site D5), the oxygen isotopic composition of product sulfate decreases compared to sulfite. With these constraints in mind, it becomes possible to compare the likelihood of various formation pathways for sulfate from each of the two sites. At site D5, incorporation of a fourth oxygen from O_2 is predicted to produce sulfate with an oxygen isotopic composition very close to the measured value of the sulfate sample from that site (**Fig. 10b**). At site D3, by contrast, incorporation of a fourth oxygen from O_2 would move the isotopic composition of product sulfate *away* from the measured value; instead, incorporation of a fourth oxygen from H_2O would produce sulfate that approaches that value (**Fig. 10a**). In other words, this analysis suggests that sulfate could be formed entirely by the oxidation of sulfite by O_2 at site D5, while the sulfate sampled from site D3 appears to require incorporation of oxygen from H_2O, possibly via Fe^{2+}-Fe^{3+} "electron shuttling" (Descostes et al., 2004; Kohl and Bao, 2011).

This representation is by necessity highly simplified; as Druschel and Borda (2006) point out, there are several possible mechanisms by which sulfate can be generated during pyrite oxidation, possibly comprising among them thousands of individual steps. One indication that

this model does not account for all relevant sulfate formation pathways is that, at site D3, even complete incorporation of H_2O oxygen (as opposed to O_2 oxygen) into sulfite produces sulfate for which the $^{18}\varepsilon_{SO_4\text{-}H_2O}$ is higher than that of the actual environmental samples (**Fig. 10a**); another process is presumably at play that accounts for that gap. Among the many other complicating factors are the rate competition between equilibrium and kinetic processes (described above) and the isotope effects involved in microbially mediated processes. A complete model of controls on the oxygen isotopic composition of sulfate produced during pyrite oxidation would need to include these factors.

Nonetheless, the relationships shown in **Fig. 10** suggest that multiple pathways are likely at play in the production of sulfate during pyrite oxidation in the natural environment. The wide variation in SO_4^{2-} oxygen isotopic composition among sites indicates that, in the natural environment as in the laboratory, no single mechanistic pathway can be invoked as an explanation. In particular, sites D3 and D5 suggest that both O_2 and H_2O are important as providers of the final oxygen to sulfite, and therefore that neither can be excluded in future investigations of this process as it manifests in natural environments. With regard to prevention strategies, these results suggest that techniques targeting specific oxidants, while potentially effective, are unlikely to prevent the formation of AMD entirely.

CONCLUSIONS

This work aims to constrain one of the many dimensions of the pyrite oxidation mechanism and apply those constraints to a natural environment, in an attempt to improve the efficacy of future acid mine drainage prevention strategies. In particular, the formation of sulfoxyanions and their equilibrium isotope effects were investigated as a means of elucidating a much-debated portion of the oxidation process.

This study has found that the aqueous sulfoxyanion intermediates sulfite and thiosulfate are not merely the transient species that they are sometimes considered to be during pyrite oxidation. Although sulfate is by far the predominant sulfoxyanion species at low pH, intermediates can accumulate in solution and even dominate the bulk sulfoxyanion pool under oxic conditions and circumneutral-to-high pH. The results presented herein suggest that simple models of aqueous equilibria are insufficient to explain the behavior of sulfoxyanions during pyrite oxidation and that other kinds of interactions, including the dynamics of attached and adsorbed sulfoxy complexes, should be considered in future work.

Due to the apparent importance of aqueous intermediate sulfoxyanions in the pyrite oxidation process, this work also aims to constrain the isotope systematics associated with these species. The equilibrium oxygen isotope fractionation factor between sulfite and water was measured under varying pH conditions, with cross-replicate averages ranging from 9.76‰ at pH 2 to 7.64‰ at pH 10. A clear dependence on sulfite species distribution was found, as $^{18}\varepsilon_{SO_3\text{-}H_2O}$ varied linearly with the logarithm of the proportion of bulk sulfite present as bisulfite. This is considered to be a result of the variation in equilibrium fractionation factors between individual sulfite species and water, which is consistent with the theoretical predictions of these values by Hemingway et al. (in preparation). The equilibrium oxygen isotope fractionation factor was also

determined for thiosulfate-water exchange at various temperatures. At 22°C, $^{18}\varepsilon_{S_2O_3\text{-}H_2O}$ ranged from a cross-replicate average of 22.11‰ at pH 2 to 14.67‰ at pH 10, reaching a minimum of 14.25‰ at pH 7. At 4°C, $^{18}\varepsilon_{S_2O_3\text{-}H_2O}$ exhibited average of 23.93‰ at pH 2 and averages of 14.43‰ and 14.74‰ at pH 7 and pH 10, respectively. Finally, at 93°C, the cross-replicate average of $^{18}\varepsilon_{S_2O_3\text{-}H_2O}$ was 13.02‰ at pH 7 and 14.25‰ at pH 10. Given the lack of appreciable speciation between thiosulfate and its protonated forms, this pH variation is unexpected and likely the result of incomplete equilibration between thiosulfate and water over the period of incubation. The value measured for pH 2 is considered the most reliable due to its close agreement with the theoretical predictions and provides a low-pH reference point for future investigations of the isotope systematics associated with thiosulfate.

Ultimately, these results were applied in an analysis of samples from a former mine site, in order to constrain the specific pathways by which sulfate is formed via pyrite oxidation in these types of environments. The calculations presented here provide support to the notion that both H_2O and O_2 are important providers of the fourth oxygen as sulfite oxidizes to sulfate, a question that underpins an ongoing debate in the literature on these topics. The model presented here is simplified, but it is clear from the widely varying oxygen isotopic composition of these sulfate samples that no single pathway is responsible for the production of sulfate. Attempts to prevent or mitigate acid mine drainage in natural environments will have to grapple with the complexity of pathways by which sulfate can form during pyrite oxidation; this work is an attempt to clarify those pathways in order to facilitate the creation of more targeted and informed prevention strategies.

REFERENCES

Abinandan, S., Venkateswarlu, K., Megharaj, M., & Subashchandrabose, S. (2018). Microalgae-bacteria biofilms: A sustainable synergistic approach in remediation of acid mine drainage. *Applied Microbiology and Biotechnology, 102*(3), 1131-1144. https://doi.org/10.1007/s00253-017-8693-7.

Akcil, A. & Koldas, S. (2006). Acid mine drainage (AMD): Causes, treatment and case studies. *Journal of Cleaner Production, 14*(12), 1139-1145. https://doi.org/j.jclepro.2004.09.006.

Baker, B.J. & Banfield, J.F. (2003). Microbial communities in acid mine drainage. *FEMS Microbiology Ecology, 44*(2), 139-152. https://doi.org/10.1016/50168-6496(03)00028-X.

Balci, N., Brunner, B., & Turchyn, A.V. (2017). Tetrathionate and elemental sulfur shape the isotope composition of sulfate in acid mine drainage. *Frontiers in Microbiology, 8*, 1564. https://doi.org/10.3389/fmicb.2017.01564.

Balci, N., Shanks, W.C., Mayer, B., & Mandernack, K.W. (2007). Oxygen and sulfur isotope systematics of sulfate produced by bacterial and abiotic oxidation of pyrite. *Geochimica et Cosmochimica Acta, 71*(15), 3796-3811. https://doi.org/10.1016/j.gca.2007.04.017.

Barnes, H.L. & Romberger, S.B. (1968). Chemical aspects of acid mine drainage. *Journal of the Water Pollution Control Federation, 40*(3), 371-384.

Basolo, F. & Pearson, R.G. (1967). Oxidation-reduction reactions. In *Mechanisms of Inorganic Reactions: A Study of Metal Complexes in Solution*, 454-525. John Wiley and Sons, New York.

Beckett, C. & Keeling, A. (2019). Rethinking remediation: Mine reclamation, environmental justice, and relations of care. *Local Environment, 24*(3), 216-230. https://doi.org/10.1080/13549839.2018.1557127.

Betts, R.H. & Voss, R.H. (1970). The kinetics of oxygen exchange between the sulfite ion and water. *Canadian Journal of Chemistry, 48*(13), 2035-2041. https://doi.org/10.1139/v70-339.

Biegler, T. & Swift, D.A. (1979). Anodic behavior of pyrite in acid solutions. *Electrochimica Acta, 24*(4), 415-420. https://doi.org/10.1016/0013-4686(79)87029-2.

Biesecker, J.E. & George, J.R. (1966). Stream quality in Appalachia as related to coal-mine drainage, 1965. U.S. Geological Survey Circular 526.

Blodau, C. (2006). A review of acidity generation and consumption in acidic coal mine lakes and their watersheds. *Science of the Total Environment, 369*(1), 307-332. https://doi.org/10.1016/j.scitotenv.2006.05.004.

Borda, M.J., Strongin, D.R., & Schoonen, M.A. (2004). A vibrational spectroscopic study of the oxidation of pyrite by molecular oxygen. *Geochimica et Cosmochimica Acta, 68*(8), 1807-1813. https://doi.org/10.1016/j.gca.2003.10.022.

Brand, W.A., Coplen, T.B., Aerts-Bijma, A.T., Böhlke, J.K., Gehre, M., et al. (2009). Comprehensive inter-laboratory calibration of reference materials for $\delta^{18}O$ versus VSMOW using various on-line high-temperature conversion techniques. *Rapid Communications in Mass Spectrometry, 23*(7), 999-1019. https://doi.org/10.1002/rcm.3958.

Brugge, D., deLemos, J.L., & Bui, C. (2007). The Sequoyah Corporation fuels release and the Church Rock spill: Unpublicized nuclear releases in American Indian communities. *American Journal of Public Health 97*(9), 1595-1600. https://doi.org/10.2105/AJPH.2006.103044.

Buzatu, A., Dill, H.G., Buzgar, N., Damian, G., Maftei, A.E., & Apopei, A.I. (2016). Efflorescent sulfates from Baia Sprie mining area (Romania) – Acid mine drainage and climatological approach. *Science of the Total Environment, 542,* 629-641. https://doi.org/j.scitotenv.2015.10.139.

Caddey, S.W., Bachman, R.L., Campbell, T.J., Reid, R.R., and Otto, R.P. (1991). The Homestake Gold Mine: An early Proterozoic iron-formation-hosted gold deposit, Lawrence County, South Dakota. *U.S. Geological Survey Bulletin 1857-J.*

Chamorro, S., Barata, C., Piña, B., Casado, M., Schwarz, A., Sáez, K., & Vidal, G. (2018). Toxicological analysis of acid mine drainage by water quality and land use bioassays. *Mine Water and the Environment, 37*(1), 88-97. https://doi.org/10.1007/s10230-017-0472-2.

Chiba, H. & Sakai, H. (1985). Oxygen isotope exchange rate between dissolved sulfate and water at hydrothermal temperatures. *Geochimica et Cosmochimica Acta, 49*(4), 993-1000. https://doi.org/10.1016/0016-7037(85)90314-X.

Cravotta, C.A. (2008). Dissolved metals and associated constituents in abandoned coal-mine discharges, Pennsylvania, USA. Part 1: Constituent quantities and correlations. *Applied Geochemistry, 23*(2), 166-202. https://doi.org/10.1016/j.apgeochem.2007.10.011.

Descostes, M., Vitorge, P., & Beaucaire, C. (2004). Pyrite dissolution in acidic media. *Geochimica et Cosmochimica Acta, 68*(22), 4559-4569. https://doi.org/10.1016/j.gca.2004.04.012.

Descostes, M., Vitorge, P., & Beaucaire, C. (2006). Response to the comment by G. Druschel and M. Borda on 'Pyrite dissolution acidic media.' *Geochimica et Cosmochimica Acta, 70*(20), 5251-5252. https://doi.org/10.1016/j.gca.2006.06.1562.

Dettrick, D., Bourgeot, N., Costelloe, J., Yuen, S., & Arora, M. (2019). The effect of particle size on mine waste sulfide oxidation rates and conceptual treatment costs. *Mine Water and the Environment, 38*(4), 735-745. https://doi.org/10.1007/s10230-019-006.

Dold, B. (2017). Acid rock drainage prediction: A critical review. *Journal of Geochemical Exploration, 172,* 120-132. https://doi.org/10.1016/j.gexplo.2016.09.014.

Druschel, G. & Borda, M. (2006). Comment on 'Pyrite dissolution in acidic media' by M. Descostes, P. Vitorge, and C. Beaucaire. *Geochimica et Cosmochimica Acta, 70*(20), 5246-5250. https://doi.org/10.1016/j.gca.2005.07.023.

Elder, J.F. (1988). Metal biogeochemistry in surface-water systems – A review of principles and concepts. U.S. Geological Survey Circular 1013.

Eldridge, D.L., Guo, W., & Farquhar, J. (2016). Theoretical estimates of equilibrium sulfur isotope effects in aqueous sulfur systems: Highlighting the role of isomers in the sulfite and sulfoxylate systems. *Geochimica et Cosmochimica Acta, 195,* 171-200. https://10.1016/j.gca.2016.09.021.

Espey, D.K., Jim, M.A., Cobb, N. et al. (2014). Leading causes of death and all-cause mortality in American Indians and Alaska Natives. *American Journal of Public Health*, *104*(S3), S303-S11. https://doi.org/10.2105/AJPH.2013.301798.

Evangelou, V.P. (2001). Pyrite microencapsulation technologies: Principles and potential field application. *Ecological Engineering*, *17*(2), 165-178. https://doi.org/10.1016/50925-8574(00)00156-7.

Evangelou, V.P., Seta, A.K., & Holt, A. (1998). Potential role of bicarbonate during pyrite oxidation. *Environmental Science & Technology*, *32*(14), 2084-2091. https://doi.org/10.1021/es970829m.

Evangelou, V.P. & Zhang, Y.L. (1995). A review: Pyrite oxidation mechanisms and acid mine drainage prevention. *Critical Reviews in Environmental Science and Technology, 25*(2), 141-199. https://doi.org/10.1080/10643389509388477.

Fernández-Remolar, D.C., Morris, R.V., Gruener, J.E., Amils, R., & Knoll, A.H. (2005). The Río Tinto Basin, Spain: Mineralogy, sedimentary geobiology, and implications for interpretation of outcrop rocks at Meridiani Planum, Mars. *Earth and Planetary Science Letters*, *240*(1), 149-167. https://doi.org/10.1016/j.epsl.2005.09.043.

Fornasiero, D., Ejit, V., & Ralston, J. (1992). An electrokinetic study of pyrite oxidation. *Colloids and Surfaces*, *62*(1-2), 63-73. https://doi.org/10.1016/0166-6622(92)80037-3.

Frantz, K. (1999). *Indian Reservations in the United States: Territory, Sovereignty, and Socioeconomic Change*. Chicago: University of Chicago Press.

Garrels, R.M. & Thompson, M.E. (1960). Oxidation of pyrite by iron sulfate solutions. *American Journal of Science, 258-A,* 57-67.

Gartman, A. & Luther, G.W. (2014). Oxidation of synthesized sub-micron pyrite (FeS_2) in seawater. *Geochimica et Cosmochimica Acta, 144,* 96-108. https://doi.org/10.1016/j.gca.2014.08.022.

Gold King Mine release (2015): USGS water-quality data and activities. (2015). *U.S. Geological Survey*. https://www.usgs.gov/mission-areas/water-resources/science/gold-king-mine-release-2015-usgs-water-quality-data-and?qt-science_center_objects=0#qt-science_center_objects. Accessed Feb. 2021.

Goldhaber, M. (1983). Experimental study of metastable sulfur oxyanion formation during pyrite oxidation at pH 6-9 and 30°C. *American Journal of Science, 283,* 193-217.

Government Accountability Office. (2020). Abandoned hardrock mines. Washington, DC. https://www.gao.gov/products/gao-20-238.

Gray, N.F. (1997). Environmental impact and remediation of acid mine drainage: A management problem. *Environmental Geology, 30*(1), 62-71. https://doi.org/10.1007/s002540050133.

Hammarstrom, J.M., Seal, R.R., Meier, A.L., & Kornfeld, J.M. (2005). Secondary sulfate minerals associated with acid drainage in the eastern US: Recycling of metals and acidity in surficial environments. *Chemical Geology, 215*(1), 407-431. https://doi.org/10.1016/j.chemgeo.2004.06.053.

Hemingway, J.D., Sutherland, K.M., Goldberg, M.G., & Johnston, D.T. (In preparation). Theoretical estimates of sulfoxyanion triple-oxygen isotope effects and their implications.

Hogsden, K.L. & Harding, J.S. (2012). Consequences of acid mine drainage for the structure and function of benthic stream communities: A review. *Freshwater Science, 31*(1), 108-120. https://doi.org/10.1899/11-091.1.

Hollings, P., Hendry, M.J., Nicholson, R.V., & Kirkland, R.A. (2001). Quantification of oxygen consumption and sulphate release rates for waste rock piles using kinetic cells: Cluff lake uranium mine, northern Saskatchewan, Canada. *Applied Geochemistry, 16*(9), 1215-1230. https://doi.org/10.1016/50883-2927(01)00005-1.

Holmes, P.R. & Crundwell, F.K. (2000). The kinetics of the oxidation of pyrite by ferric ions and dissolved oxygen: An electrochemical study. *Geochimica et Cosmochimica Acta, 64*(2), 263-274. https://doi.org/10.1016/50016-7037(99)00296-3.

Holmström, H., Ljungberg, J., & Öhlander, B. (1999). Role of carbonates in mitigation of metal release from mining waste. Evidence from humidity cells tests. *Environmental Geology, 37*(4), 267-280. https://doi.org/10.1007/s002540050384.

Huang, X. & Evangelou, V.P. (1992). Abatement of acid mine drainage by encapsulation of acid producing geologic materials. U.S. Department of the Interior, Bureau of Mines.

Jackpile-Paguate Uranium Mine: Laguna Pueblo, NM. *U.S. EPA.* https://cumulis.epa.gov/supercpad/cursites/csitinfo.cfm?id=0607033. Accessed Feb. 2021.

Jacobs, J.A., Lehr, J.H., & Testa, S.M. (2014). *Acid mine drainage, rock drainage, and acid sulfate soils: Causes, assessment, prediction, prevention, and remediation.* John Wiley & Sons, Incorporated.

Ji, M.-K., Gee, E.-D., Yun, H.-S., Lee, W.-R., Park, Y.-T., Khan, M.A., Jeon, B.-H., & Choi, J. (2012). Inhibition of sulfide mineral oxidation by surface coating agents: Batch and field studies. *Journal of Hazardous Materials, 229*(230), 298-306. https://doi.org/10.1016/j.jhazmat.2012.06.003.

Johnson, A.C., Romaniello, S.J., Reinhard, C.T., Gregory, D.D., Garcia-Robledo, E., Revsbech, N.P., Canfield, D.E., Lyons, T.W., & Anbar, A.D. (2019). Experimental determination of pyrite and molybdenite oxidation kinetics at nanomolar oxygen concentrations. *Geochimica et Cosmochimica Acta, 249,* 160-172. https://doi.org/j.gca.2019.01.022.

Johnson, D.B. & Hallberg K.B. (2005). Acid mine drainage remediation options: A review. *Science of the Total Environment, 338*(1), 3-34. https://doi.org/10.1016/j.scitotenv.2004.09.002.

Keyanna, T. (2020). Living with uranium: The impact of uranium mining on Indigenous communities. The Belfer Center, Harvard Kennedy School. Video. https://www.belfercenter.org/event/living-uranium-impact-uranium-mining-indigenous-communities.

Kleinmann, R.L.P. (1990). At-source control of acid mine drainage. *International Journal of Mine Water, 9*(1), 85-96. https://doi.org/10.1007/BF02503685.

Kohl, I. & Bao, H. (2011). Triple-oxygen-isotope determination of molecular oxygen incorporation in sulfate produced during abiotic pyrite oxidation (pH = 2-11). *Geochimica et Cosmochimica Acta, 75*(7), 1785-1798. https://doi.org/10.1016/j.gca.2011.01.003.

Le Gendre, E., Martin, E., Villemant, B., Cartigny, P., & Assayag, N. (2016). A simple and reliable anion-exchange resin method for sulfate extraction and purification suitable for multiple O- and S-isotope measurements. *Rapid Communications in Mass Spectrometry, 31*(1), 137-144. https://doi.org/10.1002/rcm.7771.

Lewis, J., Hoover, J., & MacKenzie, D. (2017). Mining and environmental health disparities in Native American communities. *Current Environmental Health Reports, 4*(2), 130-141. https://doi.org/10.1007/s40572-017-0140-5.

Li, X., Hiroyoshi, N., Tabelin, C.B., Naruwa, K., Harada, C., & Ito, M. (2019). Suppressive effects of ferric-catecholate complexes on pyrite oxidation. *Chemosphere, 214,* 70-78. https://doi.org/10.1016/j.chemosphere.2018.09.086.

Lindsay, M.B.J., Moncur, M.C., Bain, J.G., Jambor, J.L., Ptacek, C.J., & Blowes, D.W. (2015). Geochemical and mineralogical aspects of sulfide mine tailings. *Applied Geochemistry, 57,* 157-177. https://doi.org/10.1016/j.apgeochem.2015.01.009.

Lottermoser, B.G. (2010). *Mine wastes: Characterization, treatment, and environmental impacts.* Springer. https://doi.org/10.1007.978-3-642-1241.

Lowson, R.T. (1982). Aqueous oxidation of pyrite by molecular oxygen. *Chemical Reviews, 82*(5), 461-497. https://doi.org/10.1021/cr00051a001.

McKibben, M.A. & Barnes, H.L. (1986). Oxidation of pyrite in low temperature acidic solutions: Rate laws and surface textures. *Geochimica et Cosmochimica Acta, 50*(7), 1509-1520. https://doi.org/10.1016/0016-7037(86)90325-X.

Méndez-García, C., Peláez, A.I., Mesa, V., Sánchez, J., Golyshina, O.V., & Ferrer, M. (2015). Microbial diversity and metabolic networks in acid mine drainage habitats. *Frontiers in Microbiology, 6,* https://doi.org/10.3389/fmicb.2015.00475.

Millero, F.J., Hershey, P.J., Johnson, G., & Zhang, J.-Z. (1989). The solubility of SO_2 and the dissociation of H_2SO_3 in NaCl solutions. *Journal of Atmospheric Chemistry, 8*(4), 377-389. https://doi.org/10.1007/BF00052711.

Moses, C.O., Norstrom, D.K., Herman, J.S., & Mills, A.L. (1987). Aqueous pyrite oxidation by dissolved oxygen and by ferric iron. *Geochimica et Cosmochimica Acta, 51*(6), 1561-1571. https://doi.org/10.1016/0016-7037(87)90337-1.

Murphy, R. & Strongin, D. (2009). Surface reactivity of pyrite and related sulfides. *Surface Science Reports, 64*(1), 1-45. https://doi.org/10.1016/j.surfrep.2008.09.002.

New Mexico Environmental Improvement Division. (1983). The Church Rock uranium mill tailings spill: A health and environmental assessment. Santa Fe, New Mexico.

Nicholson, R.V., Gillham, R.W., & Reardon, E.J. (1988). Pyrite oxidation in carbonate-buffered solution: 1. Experimental kinetics. *Geochimica et Cosmochimica Acta, 52*(5), 1077-1085. https://doi.org/10.1016/0016-7037(88)90262-1.

Nordstrom, D.K. (2011). Mine waters: Acidic to circumneutral. *Elements, 7*(6), 393-398. https://doi.org/10.2113/gselements.7.6.393.

Nordstrom, D.K. (2015). Baseline and premining geochemical characterization of mined sites. *Applied Geochemistry, 57,* 17-34. https://doi.org/10.1016/j.apgeochem.2014.12.010.

Nordstrom, D.K., Alpers, C.N., Ptacek, C.J., & Blowes, D.W. (2000). Negative pH and extremely acidic mine waters from Iron Mountain, California. *Environmental Science & Technology, 34*(2), 254-258. https://doi.org/10.1021/es990646v.

Nordstrom, D.K., Blowes, D.W., & Ptacek, C.J. (2015). Hydrogeochemistry and microbiology of mine drainage: An update. *Applied Geochemistry, 57,* 3-16. https://doi.org/10.1016/j.apgeochem.2015.02.008.

Osburn, M.R., Kruger, B., Masterson, A.L., Casar, C.P., & Amend, J.P. (2019). Establishment of the Deep Mine Microbial Observatory (DeMMO), South Dakota, USA, a geochemically stable portal into the deep subsurface. *Frontiers in Earth Science, 7,* 196. https://doi.org/10.3389/feart.2019.00196.

Park, I. & Kim, Y. (2016). Mineralogical changes and distribution of heavy metals caused by the weathering of hydrothermally altered, pyrite-rich andesite. *Environmental Earth Sciences, 75*(15), 1125. https://doi.org/10.1007/s12665-016-5915-8.

Park, I., Tabelin, C.B., Jeon, S., Li, X., Seno, K., Ito, M., & Hiroyoshi, N. (2019). A review of recent strategies for acid mine drainage prevention and mine tailings recycling. *Chemosphere, 219,* 588-606. https://doi.org/10.1016/j.chemosphere.2018.11.053.

Park., I., Tabelin, C.B., Seno, K., Jeon, S., Ito, M., & Hiroyoshi, N. (2018). Simultaneous suppression of acid mine drainage formation and arsenic release by carrier-microencapsulation using aluminum-catecholate complexes. *Chemosphere, 205,* 414-425. https://doi.org/10.1016/j.chemosphere.2018.04.088.

Pat-Espadas, A.M., Loredo Portales, R., Amabilis-Sosa, L.E., Gómez, G., & Vidal, G. (2018). Review of constructed wetlands for acid mine drainage treatment. *Water, 10*(11), 1685. https://doi.org/10.3390/w10111685.

Powell, B. & Martens, M. (2005). A review of acid sulfate soil impacts, actions and policies that impact on water quality in Great Barrier Reef catchments, including a case study on remediation at East Trinity. *Marine Pollution Bulletin, 51*(1), 149-164. https://doi.org/10.1016/j.marpolbul.2004.10.047.

Punia, A. (2021). Role of temperature, wind, and precipitation in heavy metal contamination at copper mines: A review. *Environmental Science and Pollution Research, 28*(4), 4056-4072. https://doi.org/10.1007/s11356-020-11580-8.

Rimstidt, J.D. & Newcomb, W.D. (1993). Measurement and analysis of rate data: The rate of reaction of ferric iron with pyrite. *Geochimica et Cosmochimica Acta, 57*(9), 1919-1934. https://doi.org/10.1016/0016-7037(93)90084-A.

Rimstidt, J.D. & Vaughan, D.J. (2003). Pyrite oxidation: A state-of-the-art assessment of the reaction mechanism. *Geochimica et Cosmochimica Acta, 67*(5), 873-880. https://doi.org/10.1016/50016-7037(02)01165-1.

Rimstidt, J.D. & Vaughan, D.J. (2014). Acid mine drainage. *Elements*, 153-154.

Romano, C.G., Ulrich Mayer, K., Jones, D.R., Ellerbroek, D.A., and Blowes, D.W. (2003). Effectiveness of various cover scenarios on the rate of sulfide oxidation of mine tailings. *Journal of Hydrology, 271*(1), 171-187. https://doi.org/10.1016/S0022-1694(02)00348-7.

Rosso, K.M. & Vaughan, D.J. (2006). Reactivity of sulfide mineral surfaces. *Reviews in Mineralogy and Geochemistry, 61*(1), 557-607. https://doi.org/10.2138/rmg.2006.61.10.

RoyChowdhury, A., Sarkar, D., & Datta, R. (2015). Remediation of acid mine drainage-impacted water. *Current Pollution Reports, 1*(3), 131-141. https://doi.org/10.1007/s40726-015-0011-3.

Sánchez España, J., López Pamo, E., Santofimia, E., Aduvire, O., Reyes, J., & Barettino, D. (2005). Acid mine drainage in the Iberian Pyrite Belt (Odiel River watershed, Huelva, SW Spain): Geochemistry, mineralogy and environmental implications. *Applied Geochemistry, 20*(7), 1320-1356. https://doi.org/10.1016/j.apgeochem.2005.01.011.

Satur, J., Hiroyoshi, N., Tsunekawa, M., Ito, M., & Okamoto, H. (2007). Carrier-microencapsulation for preventing pyrite oxidation. *International Journal of Mineral Processing, 83,* 116-124. https://doi.org/10.1016/j.minpro.2007.06.003.

Schoonen, M.A.A., Harrington, A.D., Laffers, R., & Strongin, D.R. (2010). Role of hydrogen peroxide and hydroxyl radical in pyrite oxidation by molecular oxygen. *Geochimica et Cosmochimica Acta, 74*(17), 4971-4987. https://doi.org/10.1016/j.gca.2010.05.028.

Singer, P.C. & Stumm, W. (1970). Acidic mine drainage: The rate-determining step. *Science, 167*(3921), 1121-1123.

Skousen, J.G., Zipper, C.E., Rose, A., Ziemkiewicz, P.F., Nairn, R., McDonald, L.M., & Kleinmann, R.L. (2017). Review of passive systems for acid mine drainage treatment. *Mine Water and the Environment, 36*(1), 133-153. https://doi.org/10.1007/s10230-016-0417-1.

Skousen, J.G., Ziemkiewicz, P.F., & McDonald, L.M. (2019). Acid mine drainage formation, control and treatment: Approaches and strategies. *The Extractive Industries and Society, 6*(1), 241-249. https://doi.org/10.1016/j.exis.2018.09.008.

Smith, E.E. & Shumate, K. (1970). *Sulfide to Sulfate Reaction Mechanism: A Study of the Sulfide to Sulfate Reaction Mechanism as it Relates to the Formation of Acid Mine Waters.* U.S. Federal Water Quality Administration.

Steudel, R. & Steudel, Y. (2009). Microsolvation of thiosulfuric acid and its tautomeric anions $HSSO_3^-$ and $SSO_2(OH)^-$ studied by B3LYP-PCM and G3X(MP2) calculations. *The Journal of Physical Chemistry A, 113*(36), 9920-9933. https://doi.org/10.1021/jp905264c.

Tabelin, C.B., Veerawattananun, S., Ito, M., & Igarashi, T. (2017). Pyrite oxidation in the presence of hematite and alumina: I. Batch leaching experiments and kinetic modeling calculations. *Science of the Total Environment, 580,* 687-698. https://10.1016/j.scitotenv.2016.12.015.

Taylor, B.E., Wheeler, M.C., & Nordstrom, D.K. (1984). Isotope composition of sulphate in acid mine drainage as measure of bacterial oxidation. *Nature, 308*(5959), 538-541. https://doi.org/10.1038/308538a0.

Thakur Jha, R., Satur, J., Hiroyoshi, N., Ito, M., & Tsunekawa, M. (2012). Suppression of pyrite oxidation by carrier microencapsulation using silicon and catechol. *Mineral Processing & Extractive Metallurgy Review, 33*(2), 89-98. https://doi.org/10.1080/08827508.2011.562946.

The Library of Congress. A century of lawmaking for a new nation: U.S. Congressional documents and debates, 1774-1875: Statutes at large, 21st Congress, 1st session. *LOC American Memory*. https://memory.loc.gov/cgi-bin/ampage?collId=llsl&fileName=004/llsl004.db&recNum=458. Accessed Feb. 2021.

Tichomirowa, M. & Junghans, M. (2009). Oxygen isotope evidence for sorption of molecular oxygen to pyrite surface sites and incorporation into sulfate in oxidation experiments. *Applied Geochemistry, 24*(11), 2072-2092. https://doi.org/j.apgeochem.2009.08.002.

Toran, L. (1987). Sulfate contamination in groundwater from a carbonate-hosted mine. *Journal of Contaminant Hydrology, 2*(1), 1-29. https://10.1016/0169-7722(87)90002-7.

Toran, L. & Harris, R.F. (1989). Interpretation of sulfur and oxygen isotopes in biological and abiological sulfide oxidation. *Geochimica et Cosmochimica Acta, 53*(9), 2341-2348. https://doi.org/10.1016/0016-7037(89)90356-6.

Townsend, M. (1989). Congressional abrogation of Indian treaties: Reevaluation and reform. *Yale Law Review 98*(4), 793-812. https://www.jstor.org/stable/796733.

Turkewitz, J. (Aug. 16, 2016). Navajo Nation sues E.P.A. in poisoning of a Colorado river. *New York Times.*

United Nuclear Corp. foresees a rise in need for power plants. (July 18, 1970). *New York Times.* ProQuest.

U.S. Congress, House of Representatives, Committee on Interior and Insular Affairs. (1979). *Mill Tailings Dam Break at Church Rock, New Mexico*. 96th Congress, 1st sess.

U.S. Congress. (1919). *Public Laws of the Sixty-Sixth Congress.* 66th Congress, 1st sess. Ch. 4.

U.S. Environmental Protection Agency. (1994). Technical document: Acid mine drainage prediction. U.S. EPA Office of Solid Waste.

Van Stempvoort, D.R. & Krouse, H.R. (1994). Environmental geochemistry of sulfide oxidation. In *Controls of ^{18}O in Sulfate.* American Chemical Society: Salem, MA.

Voyles, T.B. (2015). *Wastelanding: Legacies of Uranium Mining in Navajo Country*. Minneapolis: University of Minnesota Press.

Wankel, S.D., Bradley, A.S., Eldridge, D.L., & Johnston, D.T. (2014). Determination and application of the equilibrium oxygen isotope effect water and sulfite. *Geochimica et Cosmochimica Acta, 125,* 694-711. https://doi.org/10.1016/j.gca.2013.08.039.

Wiersma, C.L. & Rimstidt, J.D. (1984). Rates of reaction of pyrite and marcasite with ferric iron at pH 2. *Geochimica et Cosmochimica Acta, 48*(1), 85-92. https://doi.org/10.1016/0016-7037(84)90351-X.

Williamson, M.A., Kirby, C.S., & Rimstidt, J.D. (2006). Iron dynamics in acid mine drainage. *Journal of the American Society of Mining and Reclamation,* 2, 2411-2423. https://doi.org/10.21000/JASMR06022411.

Williamson, M.A. & Rimstidt, J.D. (1993). The rate of decomposition of the ferric-thiosulfate complex in acidic aqueous solutions. *Geochimica et Cosmochimica Acta, 57*(15), 3555-3561. https://doi.org/10.1016/0016-7037(93)90138-M.

Williamson, M.A. & Rimstidt, J.D. (1994). The kinetics and electrochemical rate-determining step of aqueous pyrite oxidation. *Geochimica et Cosmochimica Acta, 58*(24), 5443-5454. https://doi.org/10.1016/0016-7037(94)90241-0.

Xu, Y. & Schoonen, M.A.A. (1995). The stability of thiosulfate in the presence of pyrite in low-temperature aqueous solutions. *Geochimica et Cosmochimica Acta, 59*(22), 4605-4622. https://doi.org/10.1016/0016-7037(95)00331-2.